NASA TECHNICAL NOTE

NASA TN D-2102

c. 1

NASA TN D-2102

ANALYTICAL INVESTIGATION OF REDUCTION IN TURBULENT SKIN FRICTION ON A FLAT PLATE BY MEANS OF AIR INJECTION THROUGH DISCRETE SLOTS

by K. R. Czarnecki

Langley Research Center
Langley Station, Hampton, Va.

NATIONAL AERONAUTICS AND SPACE ADMINISTRATION • WASHINGTON, D. C. • NOVEMBER 1964

ANALYTICAL INVESTIGATION OF REDUCTION IN TURBULENT SKIN FRICTION ON A FLAT PLATE BY MEANS OF AIR INJECTION THROUGH DISCRETE SLOTS

By K. R. Czarnecki

Langley Research Center
Langley Station, Hampton, Va.

NATIONAL AERONAUTICS AND SPACE ADMINISTRATION

For sale by the Office of Technical Services, Department of Commerce, Washington, D.C. 20230 -- Price $1.50

ANALYTICAL INVESTIGATION OF REDUCTION IN TURBULENT SKIN FRICTION ON A FLAT PLATE BY MEANS OF AIR INJECTION THROUGH DISCRETE SLOTS

By K. R. Czarnecki
Langley Research Center

SUMMARY

An analytical investigation based on a number of simplifying assumptions has been made of the possibilities of reduction in compressible turbulent skin friction on a flat plate by means of low-energy air injection through discrete slots. The analysis is based on the combination of the momentum losses in the boundary-layer and injection-air flows, and employs the Sommer and Short reference temperature method for estimating boundary-layer skin friction.

The results of the analysis indicate that the greatest theoretical reductions in skin friction occurred at the lowest injection-air pressure recovery factors defined as the fraction of free-stream dynamic pressure energy still preserved in the injection engine or bleed air after entrance losses, and thus at the lowest air injection velocities. For the optimum set of conditions considered in the analysis, the maximum reduction in skin friction at a Mach number of 3 was about 24 percent at a recovery factor of 0.005. For an anticipated pressure recovery range of 0.25 to 0.50, the calculated reduction in skin friction with the remaining conditions being held constant was on the order of 10 to 5 percent. In general, increases in free-stream Mach number, increases in free-stream Reynolds number per foot, internal heating of the bleed air, and movement of the injection slot downstream from the leading edge led to decreases in the available reductions in skin friction; whereas, internal cooling of the bleed air, increases in chord length at constant injection mass flow, and increases in injection-air mass flow resulted in increases in the amount of reduction in skin friction that is possible. Pressure losses in injection-air ducting rapidly negated the favorable effects of air injection.

INTRODUCTION

The successful development of a long-range supersonic transport airplane is critically dependent upon the attainment of reasonably high lift-drag ratios. Inasmuch as boundary-layer skin friction constitutes a substantial portion of the overall drag of an airplane of efficient design, one method of obtaining the desired ratios is to reduce the skin friction of the turbulent boundary layer, which covers most of the airplane surfaces, to values below those normally found on a smooth surface. This reduction can be accomplished by the injection of low-energy air into the boundary layer. Engine bleed air or spent cabin air could serve as a source of this low-energy air.

Two possible methods of injecting air into the boundary layer are generally being considered. In the first method, air is injected continuously over the complete area of interest through a porous surface. Reduction in skin friction in this approach is achieved primarily by an alteration or distortion of the boundary-layer profile such that the velocity gradient perpendicular to the surface, which is a direct measure of the local skin friction, is reduced. A further, but smaller, decrease in skin friction results from the forced thickening of the boundary layer, inasmuch as thicker boundary layers of the same basic profile also cause a decrease in the absolute boundary-layer velocity gradients. In the second method, low-energy air is injected into the boundary layer by means of discrete slots, and reduction in skin friction is realized primarily from the forced thickening of the boundary layer. This forced thickening is usually initiated close to the origin of the turbulent boundary layer.

The method of injection through porous surfaces is aerodynamically more efficient (if the pressure losses through the porous surface are excluded) and has been studied in considerable detail (see refs. 1 to 5, for example). However, the method poses prodigious design problems for adaptation to practical use because porous skins tend to be weak and brittle, have high resistance to air flows, and clog very easily, and because of the difficulty of attaining access to large areas of surface with the air on the usual airplane. The discrete-slot technique, on the other hand, although aerodynamically less efficient, has no clogging problem and is more readily amenable to practical design. Little has been done, however, to investigate the potential gains from the latter type of approach. The present analytical investigation was undertaken to fulfill the need for information in this area and to serve as a guide for experimental research.

The basic objectives of this investigation were to determine the magnitudes of skin-friction reduction that might be possible with low-energy air injection by discrete slots and to relate the reductions to slot location, injection-air mass flow, engine bleed air pressure recovery, chord length, and heat transfer for a range of Mach numbers and Reynolds numbers. Effects of ducting pressure losses on the efficiency of this method of skin-friction reduction were also studied.

The analysis is based on the combination of the momentum losses in the boundary-layer and injection-air mass flows, and employs the Sommer and Short reference temperature method for estimating boundary-layer skin friction. (See ref. 6.)

SYMBOLS

Dimensional:

a	speed of sound
c	chord length of basic flat plate
c_p	specific heat of air at constant pressure
l	leading edge
ls	distance from leading edge to slot
ls'	fictitious distance from leading edge to slot after inclusion of effects of air injection
m	mass flow of air
m_e	mass flow of air injected through slot per unit span, $\rho_e u_e w$
m_∞	reference mass flow of air, $\rho_\infty u_\infty c$
p	pressure (static pressure when used without subscript t)
q	dynamic pressure, $\frac{\gamma}{2} pM^2$
R	perfect gas constant
R_{ft}	free-stream Reynolds number per foot, $\frac{\rho_\infty u_\infty}{\mu_\infty}$
S	Sutherland gas constant
s	slot location
s'	effective slot location
ss'	fictitious increase in length of boundary layer or displacement distance resulting from air injection
$s't'$	fictitious distance from slot to trailing edge of flat plate after inclusion of effects of air injection
T	absolute temperature (static temperature when used without subscript t)
T'	reference temperature $\left(\frac{T'}{T_\infty} = 1 + 0.035M_\infty^2 + 0.45\left(\frac{T_w}{T_\infty} - 1\right)\right)$

t	trailing edge
t'	effective trailing edge
u	velocity parallel to surface in stream direction
w	width of injection-air slot
x	longitudinal distance along surface from leading edge
γ	ratio of specific heat at constant pressure to specific heat at constant volume
δ	total boundary-layer thickness
δ^*	boundary-layer displacement thickness, $\int_0^\delta \left(1 - \frac{\rho u}{\rho_\infty u_\infty}\right)dy$
θ	boundary-layer momentum thickness, $\int_0^\delta \frac{\rho u}{\rho_\infty u_\infty}\left(1 - \frac{u}{u_\infty}\right)dy$
μ	absolute viscosity of air
μ'	absolute viscosity of air at reference temperature; $\frac{\mu'}{\mu_\infty} = \left(\frac{T'}{T_\infty}\right)^{3/2}\left(\frac{T_\infty + S}{T' + S}\right)$
ρ	mass density of air

Dimensionless parameters:

A	Reynolds number transfer parameter, $\frac{1}{\left(\frac{T'}{T_\infty}\right)\left(\frac{\mu'}{\mu_\infty}\right)}$
C_D	total drag coefficient, $\frac{\text{Friction drag + Drag due to ducting pressure losses}}{q_\infty x}$
C_F	average skin-friction coefficient, $\frac{\text{Friction drag}}{q_\infty x}$
$\frac{\Delta C_D}{C_{F_{lt}}}$	reduction in total drag parameter (defined by eq. (47))
$\frac{\Delta C_F}{C_{F_{lt}}}$	reduction in skin-friction parameter (defined by eq. (11))

H	boundary-layer shape parameter, $\frac{\delta^*}{\theta}$
$\frac{l_s}{c}$	slot-location ratio
M	Mach number, u/a, or $\frac{u}{\sqrt{\gamma RT}}$
$\frac{m_e}{m_\infty}$	mass-flow ratio
m^*	mass-flow parameter, $\frac{m_e/m_\infty}{w/c}$
R_∞	Reynolds number, $\frac{\rho_\infty u_\infty x}{\mu_\infty}$
r	pressure recovery factor, $\frac{p_{t,e} - p_\infty}{p_{t,\infty} - p_\infty}$
$\frac{ss'}{c}$	displacement distance parameter
$\frac{T_{t,e}}{T_{t,\infty}}$	injection-air temperature ratio
$\frac{u_e}{u_\infty}$	injection-air or exit velocity ratio
$\frac{w}{c}$	slot-width to chord ratio
$\frac{\Delta\theta_{ss'}}{c}$	incremental boundary-layer momentum thickness ratio
θ^*	incremental boundary-layer momentum thickness parameter, $\frac{\frac{\Delta\theta_{ss'}}{c}}{w/c}$ or $\frac{\Delta\theta_{ss'}}{w}$

Subscripts:

bl	boundary layer
d	including effects of injection air-ducting pressure losses
e	located at slot exit
e,d	located at slot exit but including effects of ducting pressure losses

ls	from leading edge to slot location
ls'	from leading edge to fictitious slot location after inclusion of effects of air injection
lt	from leading to trailing edge of basic flat plate
lt'	from leading edge to fictitious trailing edge of flat plate after inclusion of effects of air injection
M_e	Mach number at exit of slot
max	maximum
s	located just ahead of slot
s'	located just behind slot
ss'	increment due to injection of air
s't'	from slot to fictitious trailing edge of flat plate after inclusion of effects of air injection
t	stagnation
t,e	stagnation in injection-air flow
t,∞	stagnation in free-stream flow
w	wall
θ^*_{max}	conditions for which θ^* is maximum
∞	free stream
35	chord of 35 feet

A bar over a symbol denotes quantities to be computed with the aid of a modified wall temperature.

ANALYSIS

Equation for Reduction of Skin Friction

If low-energy air is injected into a turbulent boundary layer, it will mix with the boundary layer and increase the boundary-layer thickness. If the boundary-layer profile is not distorted, the increased thickness will reduce the velocity gradients through the boundary layer perpendicular to the surface and, because the magnitude of the velocity gradient at the surface is a direct indicator of the local skin friction, the boundary-layer skin friction will be reduced. If the air injection is sufficiently close to the wing or body leading edge and is achieved without the creation of undue flow disturbances, then relatively large segments of the airplane surfaces can be sheathed in this thickened boundary-layer flow and significant reductions in skin-friction drag may be realized.

In order to simplify the analysis the following assumptions are made:

(1) The flow is two dimensional

(2) The boundary layer is on a sharp-edged flat plate, and the pressure gradient in the flow direction is zero

(3) Turbulent boundary-layer flow originates at the plate leading edge

(4) Air is injected into the boundary layer through a discrete slot having a width sufficiently narrow relative to the flat-plate chord so that the loss in surface area represented by the slot can be neglected

(5) Air is injected into the boundary layer in a direction parallel to the free stream

(6) Boundary-layer-air and injection-air mixing is rapid, and the new thickened boundary layer assumes its new equilibrium velocity profile immediately upon air injection

(7) Air injection can be accomplished without the creation of undue external flow disturbances.

The starting point of the analysis is the well-known relationship between the boundary-layer average skin-friction coefficient C_F and the boundary-layer momentum thickness θ in two-dimensional flat-plate flow expressed by

$$C_F = \frac{2\theta}{x} \tag{1}$$

For the case where there is no air injection, the momentum thickness will grow proportionally approximately as the four-fifths power of the distance from the plate leading edge as illustrated in the upper part of figure 1. When low-energy air injection is present, the momentum thickness will increase abruptly at the point of injection and then the momentum thickness will resume its normal rate of increase as indicated in the lower part of figure 1. Because of the increased boundary-layer thickness, the normal rate of increase is now slower than it is without air injection, and the skin friction to the rear of the slot location is decreased.

For the case where the enthalpy or stagnation temperature of the injected air is equal to that of the free stream, as will be the situation where there is no heat transfer and where engine bleed air is not used for any purpose other than injection into the boundary layer, there will be no change in the ratio of surface temperature to free-stream temperature behind the slot involving heat transfer, and the method of estimating the reduction in skin friction becomes readily apparent. In effect, the rate of momentum thickness increase behind the slot can now be equated to that of a boundary layer of equal thickness displaced downstream of the slot location by a distance ss' on a flat plate whose chord has also been extended by the distance ss'. The increase in momentum thickness $\Delta\theta_{ss'}$ induced by the air injection is not chargeable to skin friction. Consequently, the skin friction on the flat plate with air injection (lower part of fig. 1) is now equivalent to the skin friction existing on the fictitious extended plate (upper part of fig. 1) in the regions ls and $s't'$.

In equation form, the increment in skin-friction reduction resulting from air injection can be expressed as

$$\frac{\Delta C_F}{C_{F_{lt}}} = -\frac{C_{F_{lt}} - \left[C_{F_{lt'}}\left(\frac{c + ss'}{c}\right) - C_{F_{ls'}}\left(\frac{ls + ss'}{c}\right) + C_{F_{ls}}\left(\frac{ls}{c}\right)\right]}{C_{F_{lt}}} \tag{2}$$

or

$$\frac{\Delta C_F}{C_{F_{lt}}} = \frac{C_{F_{lt'}}}{C_{F_{lt}}}\left(\frac{c + ss'}{c}\right) - \frac{C_{F_{ls'}}}{C_{F_{lt}}}\left(\frac{ls + ss'}{c}\right) + \frac{C_{F_{ls}}}{C_{F_{lt}}}\left(\frac{ls}{c}\right) - 1 \tag{3}$$

where the increment has been normalized by the skin friction existing on the flat plate before injection, and the sign convention has been adopted in which a negative increment represents a reduction in skin friction and a positive increment an increase. With the aid of equation (1) it is established that

$$C_{F_{ls'}} = \frac{2}{ls'}\left(\frac{ls}{2} C_{F_{ls}} + \Delta\theta_{ss'}\right) \tag{4}$$

Substitution of equation (4) into equation (3) gives, after some manipulation,

$$\frac{\Delta C_F}{C_{F_{lt}}} = \left(1 + \frac{ss'}{c}\right)\frac{C_{F_{lt'}}}{C_{F_{lt}}} - \frac{2}{C_{F_{lt}}}\frac{\Delta\theta_{ss'}}{c} - 1 \tag{5}$$

For the case where the enthalpy or stagnation temperature of the injection air is not identical to that of the free stream, as will be true in installations where the engine bleed air is first used for engine accessory or cabin cooling before injection into the boundary layer or where spent cabin air is utilized, there is an additional change in skin friction downstream of the slot that cannot be incorporated into equation (5) without some qualifications. This is the change in skin friction resulting from the relative change in heat-transfer potential in this area. This additional heat-transfer effect can be approximated by the use of a modified wall temperature (to be discussed in a later section) that is applied to the complete length of the fictitious extended plate. In order to make the application, it is necessary to extend or contract the distance from plate leading edge to slot location ls by a correction distance $\overline{\Delta l s}$, so that the momentum thickness just ahead of the slot is not changed by the addition or subtraction of heat energy in the new calculations.

In equation form the change in skin friction in the area of $s't'$ resulting from the differences in injection-air and free-stream stagnation temperatures can be expressed as

$$-\frac{\overline{\Delta C_{F_{s't'}}}}{C_{F_{lt}}} = \left[\frac{C_{F_{lt'}}}{C_{F_{lt}}}\left(\frac{c + ss'}{c}\right) - \frac{C_{F_{ls'}}}{C_{F_{lt}}}\left(\frac{ls + ss'}{c}\right)\right] - \left[\frac{\overline{C_{F_{lt'}}}}{C_{F_{lt}}}\left(\frac{c + \overline{\Delta ls} + \overline{ss'}}{c}\right) - \frac{\overline{C_{F_{ls}}}}{C_{F_{lt}}}\left(\frac{\overline{ls} + \overline{ss'}}{c}\right)\right] \tag{6}$$

where the minus sign is applied to the increment to fit within the previously adopted sign convention for positive and negative reduction in skin friction. The barred quantities denote values computed with the aid of the new or modified wall temperature; those without bars are determined for conditions of equal stagnation temperatures for injection-air and free-stream flow. The correction distance $\overline{\Delta ls}$ can be found with the aid of equation (1) as follows:

$$ls C_{F_{ls}} = (ls + \overline{\Delta ls})\overline{C_{F_{ls}}} \tag{7}$$

and

$$\overline{\Delta ls} = ls\left(\frac{C_{F_{ls}}}{\overline{C_{F_{ls}}}} - 1\right) \tag{8}$$

where all the quantities on the right-hand side of equation (8) are known or are calculable. With the use of equation (4) and its counterpart for the case of the unequal stagnation temperatures, along with the utilization of equation (7), equation (6) is converted to

$$\frac{\overline{\Delta C_{F_{s't'}}}}{C_{F_{lt}}} = \frac{\overline{C_{F_{lt'}}}}{C_{F_{lt}}}\left(\frac{c + \overline{\Delta ls} + \overline{ss'}}{c}\right) - \frac{C_{F_{lt'}}}{C_{F_{lt}}}\left(\frac{c + ss'}{c}\right) - \frac{2}{C_{F_{lt}}}\left(\frac{\overline{\Delta\theta_{ss'}}}{c} - \frac{\Delta\theta_{ss'}}{c}\right) \tag{9}$$

Addition of equations (5) and (9) gives

$$\frac{\Delta C_F + \overline{\Delta C_{F_{s't'}}}}{C_{F_{lt}}} = \frac{C_{F_{lt'}}}{C_{F_{lt}}}\left(1 + \frac{\overline{\Delta ls}}{c} + \frac{\overline{ss'}}{c}\right) - \frac{2}{C_{F_{lt}}}\frac{\overline{\Delta\theta_{ss'}}}{c} - 1 \tag{10}$$

In equation (10) the quantity $\frac{\overline{\Delta\theta_{ss'}}}{c}$ is independent of any external heat-transfer or Reynolds number effects (as will be developed subsequently), and the two increments $\frac{\Delta C_F}{C_{F_{lt}}}$ and $\frac{\overline{\Delta C_{F_{s't'}}}}{C_{F_{lt}}}$ can be determined in combination in a single step by the proper management of the other pertinent quantities. Equation (10), therefore, can be simplified to

$$\frac{\Delta C_F}{C_{F_{lt}}} = \frac{\overline{C_{F_{lt'}}}}{C_{F_{lt}}}\left(1 + \frac{\overline{\Delta ls}}{c} + \frac{\overline{ss'}}{c}\right) - \frac{2}{C_{F_{lt}}} \frac{\Delta\theta_{ss'}}{c} - 1 \tag{11}$$

where the bars have been dropped for convenience from all quantities except those on the right-hand side of the equation which must be computed with the aid of the new or modified wall temperature. The quantity $\frac{\Delta\theta_{ss'}}{c}$, of course, must be computed for the proper value of $\frac{T_{t,e}}{T_{t,\infty}}$. For equal stagnation temperatures $\frac{\Delta ls}{c} = 0$, and equation (11) reverts to equation (5).

Determination of $\frac{\Delta\theta_{ss'}}{c}$

The quantity of prime importance in equations (5) and (11) is $\frac{\Delta\theta_{ss'}}{c}$, because it is related directly to the problems of air injection or reduction in skin friction. This quantity is found by the use of the basic definition for the boundary-layer momentum thickness in two-dimensional compressible flow

$$\theta \equiv \int_0^{\delta} \frac{\rho u}{\rho_\infty u_\infty}\left(1 - \frac{u}{u_\infty}\right)dy \tag{12}$$

The increase in boundary-layer momentum thickness caused by air injection is found by subtracting the momentum thickness just ahead of the slot from that just behind the slot after injection

$$\theta_{s'} - \theta_s = \Delta\theta_{ss'} = \int_0^{\delta_{s'}} \frac{\rho u}{\rho_\infty u_\infty}\left(1 - \frac{u}{u_\infty}\right)dy - \int_0^{\delta_s} \frac{\rho u}{\rho_\infty u_\infty}\left(1 - \frac{u}{u_\infty}\right)dy \tag{13}$$

With the use of the theorems of conservation of mass and of momentum, along with the use of the definition

$$\frac{m_e}{m_\infty} \equiv \frac{\rho_e u_e w}{\rho_\infty u_\infty c} \tag{14}$$

equation (13) converts into

$$\frac{\Delta\theta_{ss'}}{c} = \frac{m_e}{m_\infty}\left(1 - \frac{u_e}{u_\infty}\right) \tag{15}$$

In order to find an expression for u_e/u_∞ in terms of some readily known basic quantities, equation (14) is solved for

$$\frac{u_e}{u_\infty} = \frac{m_e/m_\infty}{w/c}\,\frac{\rho_\infty}{\rho_e} = m^*\,\frac{\rho_\infty}{\rho_e} \tag{16}$$

where

$$m^* \equiv \frac{m_e/m_\infty}{w/c} \tag{17}$$

If the assumption is made that the static pressure in the slot exit is equal to free-stream static pressure (that is, $p_e = p_\infty$), then the thermal equation of state indicates

$$\frac{\rho_\infty}{\rho_e} = \frac{T_e}{T_\infty} \tag{18}$$

In general, T_e will not be known directly but can be found readily from the energy equation

$$T_e = T_{t,e} - \frac{u_e^2}{2c_p} \tag{19}$$

if the stagnation temperature $T_{t,e}$ of the injected air is known. For flight conditions T_∞ will usually be one of the basic known quantities. Substitution of equations (18) and (19) into equation (16) gives the equation

$$\frac{u_e}{u_\infty} = m^*\left[\frac{T_{t,e}}{T_\infty} - \frac{\gamma - 1}{2} M_\infty^{\;2}\left(\frac{u_e}{u_\infty}\right)^2\right] \tag{20}$$

Equation (20) is a quadratic, and its solution by the usual method yields

$$\frac{u_e}{u_\infty} = \frac{-\frac{1}{m^*} + \sqrt{\left(\frac{1}{m^*}\right)^2 + 4\left(\frac{\gamma - 1}{2} M_\infty^2\right)\left(\frac{T_{t,e}}{T_\infty}\right)}}{2\left(\frac{\gamma - 1}{2} M_\infty^2\right)} \tag{21}$$

because only the plus sign for the radical has any physical meaning. Introduction of equation (21) into equation (15) produces the desired equation

$$\theta^* = m^* + \frac{1}{2\left(\frac{\gamma - 1}{2} M_\infty^2\right)}\left[1 - \sqrt{1 + 4m^{*2}\left(\frac{\gamma - 1}{2} M_\infty^2\right)\frac{T_{t,e}}{T_\infty}}\right] \tag{22}$$

where

$$\theta^* = \frac{\frac{\Delta\theta_{ss'}}{c}}{w/c} = \frac{\Delta\theta_{ss'}}{w} \tag{23}$$

and where all quantities on the right-hand side of the expression are known or are readily calculable. For wind-tunnel usage the equation is converted to

$$\theta^* = m^* + \frac{1}{2\left(\frac{\gamma - 1}{2} M_\infty^2\right)}\left[1 - \sqrt{1 + 4m^{*2}\left(\frac{\gamma - 1}{2} M_\infty^2\right)\left(1 + \frac{\gamma - 1}{2} M_\infty^2\right)\frac{T_{t,e}}{T_{t,\infty}}}\right] \tag{24}$$

For $M_\infty = 0$, equations (22) and (24) reduce to

$$\theta^* = m^*\left(1 - m^* \frac{T_{t,e}}{T_{t,\infty}}\right) \tag{25}$$

Determination of Skin-Friction Coefficients

The calculations for the reduction in skin friction due to air injection can be accomplished, of course, with the use of any one of the theories available for the turbulent boundary layer. Most recent studies have tended to favor the use of one of the so-called T' or reference temperature methods. (For example, see ref. 7.) In this investigation the T' method of Sommer and Short (ref. 6), utilizing Schlichting's simplification of the Kármán-Schoenherr incompressible-flow curve, is used.

In the method chosen, the skin-friction coefficient in compressible flow is given by

$$C_F = 0.46 \frac{T_\infty}{T'}\left(\log_{10}A + \log_{10}R_{ft} + \log_{10}x\right)^{-2.6} \tag{26}$$

where for convenience the Reynolds number R_∞ has been divided into its components R_{ft} and x.

In order to apply equation (26) to equations (5) and (11), the x in equation (26) must be replaced by the proper length. Thus, to find $C_{F_{lt}}$ the equation is modified to

$$C_{F_{lt}} = 0.46 \frac{T_\infty}{T'}\left(\log_{10}A + \log_{10}R_{ft} + \log_{10}c\right)^{-2.6} \tag{27}$$

To find $\overline{C_{F_{lt'}}}$ equation (26) is converted to

$$\overline{C_{F_{lt'}}} = 0.46\left(\overline{\frac{T_\infty}{T'}}\right)\left[\log_{10}\bar{A} + \log_{10}R_{ft} + \log_{10}\left(c + \overline{\Delta ls} + \overline{ss'}\right)\right]^{-2.6} \tag{28}$$

wherein the effects of $\frac{T_{t,e}}{T_{t,\infty}} \neq 1$ can be incorporated by the use of a modified wall temperature T_w. Thus, with the aid of equations (4) and (26) an expression relating $\overline{ss'}$ with $\theta_{ss'}$ is obtained, which is

$$\begin{aligned}\frac{\theta_{ss'}}{c} = {} & 0.23\left(\frac{ls}{c} + \frac{\overline{\Delta ls}}{c} + \frac{\overline{ss'}}{c}\right)\left(\overline{\frac{T_\infty}{T'}}\right)\left[\log_{10}\bar{A} + \log_{10}R_{ft} + \log_{10}\left(ls + \overline{\Delta ls} + \overline{ss'}\right)\right]^{-2.6} \\ & -0.23\left(\frac{ls}{c} + \frac{\overline{\Delta ls}}{c}\right)\left(\overline{\frac{T_\infty}{T'}}\right)\left[\log_{10}\bar{A} + \log_{10}R_{ft} + \log_{10}\left(ls + \overline{\Delta ls}\right)\right]^{-2.6}\end{aligned} \tag{29}$$

Before equation (29) can be utilized, methods for establishing the term $\overline{\Delta ls}$ and the fictitious or modified wall temperature must be devised. With the help of equations (8) and (26) the relation required to determine $\overline{\Delta ls}$ is found to be

$$\overline{\Delta ls} = ls\left\{\frac{\left(\overline{\frac{T_\infty}{T'}}\right)}{\left(\frac{T_\infty}{T'}\right)}\left[\frac{\log_{10}\bar{A} + \log_{10}R_{ft} + \log_{10}\left(ls + \overline{\Delta ls}\right)}{\log_{10}A + \log_{10}R_{ft} + \log_{10}ls}\right]^{2.6} - 1\right\} \tag{30}$$

Unfortunately, equation (30) cannot be solved for $\overline{\Delta ls}$ explicitly. The best procedure is to insert a set of arbitrary values of $\overline{\Delta ls}$ in the equation and solve for the corresponding values of $\overline{\left(\frac{T_\infty}{T'}\right)}$. A plot is made of $\overline{\Delta ls}$ as a function of $\overline{\left(\frac{T_\infty}{T'}\right)}$, and then used to pick values of $\overline{\Delta ls}$ for known values of $\overline{\left(\frac{T_\infty}{T'}\right)}$.

The term $\overline{\left(\frac{T_\infty}{T'}\right)}$ is derived from the reference temperature equation (ref. 6)

$$\frac{T'}{T_\infty} = 1 + 0.035 M_\infty^{\ 2} + 0.45\left(\frac{T_w}{T_\infty} - 1\right) \tag{31}$$

with the use of a modified T_w $\left(\text{or } \overline{T_w}\right)$. In veiw of the many simplifying assumptions already incorporated into the theory, a relatively crude but simple method of estimating the term $\overline{\left(\frac{T_\infty}{T'}\right)}$ was used. The assumption was made that the average wall temperatures behind the injection slot could be determined from the relative mass flows in the boundary layer and injection slots and their corresponding stagnation temperatures as indicated in the following equation:

$$\overline{T_w} = \frac{T_w m_{bl} + T_w \frac{T_{t,e}}{T_{t,\infty}} m_e}{m_{bl} + m_e} \tag{32}$$

In equation (32) T_w is the surface temperature that would exist in the absence of air injection, m_{bl} is the average value of the mass flow in the boundary layer between the slot and the plate trailing edge without injection, and m_e is the mass flow through the slot. Application to equation (32) of equations (1) and (26) along with the definitions

$$\frac{\rho_\infty u_\infty \delta^*}{\rho_\infty u_\infty c} \equiv \frac{m_{bl}}{m_\infty} = \frac{\delta^*}{c} \tag{33}$$

$$H \equiv \frac{\delta^*}{\theta} \tag{34}$$

leads to

$$\bar{T}_w = T_w \left[\frac{\frac{H}{4}\left(C_{F_{lt}} + C_{F_{ls}} \frac{ls}{c}\right) + \frac{T_{t,e}}{T_{t,\infty}} \frac{m_e}{m_\infty}}{\frac{H}{4}\left(C_{F_{lt}} + C_{F_{ls}} \frac{ls}{c}\right) + \frac{m_e}{m_\infty}}\right] \tag{35}$$

The value of the boundary-layer shape parameter H can be determined as a function of free-stream Mach number in reference 8.

Inspection of equation (29) at this point reveals that $\frac{\overline{ss'}}{c}$ or $\frac{ss'}{c}$ cannot be found explicitly. A procedure similar to that for finding $\overline{\Delta ls}$ must be adopted.

Pressure Recovery Factor

One of the most desirable, and probably essential, features of an efficient air-injection system for an airplane is that the desired injection-air mass flows and velocities be attained without the use of auxiliary devices other than a throttle. Thus, it becomes desirable to relate the injection mass flows and velocities to the ram or recovery pressure that might be available in the engine bleed or spent cabin air. This relationship is accomplished by first converting equation (16) with the aid of the thermal equation of state to $\left(p_e = p_\infty\right.$ being assumed$\left.\right)$

$$\frac{u_e}{u_\infty} = m^* \frac{T_e}{T_\infty} \tag{36}$$

With the use of the energy equation (eq. (19)), equation (36) is reduced to

$$\frac{u_e}{u_\infty} = \sqrt{\frac{T_{t,e} - T_e}{T_{t,\infty} - T_\infty}} \tag{37}$$

Substitution of equation (37) in equation (15) results in

$$\frac{\Delta\theta_{ss'}}{c} = \frac{m_e}{m_\infty}\left(1 - \sqrt{\frac{T_{t,e} - T_e}{T_{t,\infty} - T_\infty}}\right) \tag{38}$$

Inasmuch as $p_e = p_\infty$, it can be established that

$$\frac{T_e}{T_\infty} = \frac{T_{t,e}}{T_{t,\infty}}\left(\frac{p_{t,\infty}}{p_{t,e}}\right)^{\frac{\gamma-1}{\gamma}} \tag{39}$$

and, hence, elimination of temperature ratios yields

$$\theta^* = m^* - \frac{1}{\frac{\gamma - 1}{2} M_\infty^2}\left[\left(1 + \frac{\gamma - 1}{2} M_\infty^2\right)\left(\frac{p_{t,e}}{p_{t,\infty}}\right)^{\frac{\gamma-1}{\gamma}} - 1\right] \tag{40}$$

Equation (40) is compatible with equation (24) only for equal values of θ^* or m^*. Furthermore, because the ram pressure of the bleed air must satisfy the condition

$$p_\infty < p_{t,e} < p_{t,\infty}$$

as a result of the basic assumptions inherent in the analysis (and pressure of the cabin air, too, for practical reasons), it is possible to introduce a recovery factor r defined by

$$r = \frac{p_{t,e} - p_\infty}{p_{t,\infty} - p_\infty} \tag{41}$$

Consequently, equating the right-hand parts of equations (24) and (40), along with the use of equation (41), yields

$$m^* = \sqrt{\frac{\left\{\left[r\left(1 + \frac{\gamma - 1}{2} M_\infty^2\right)^{\frac{\gamma}{\gamma-1}} - r + 1\right]^{\frac{\gamma-1}{\gamma}} - \frac{1}{2}\right\}^2 - \frac{1}{4}}{\left(\frac{\gamma - 1}{2} M_\infty^2\right)\left(1 + \frac{\gamma - 1}{2} M_\infty^2\right)\left(\frac{T_{t,e}}{T_{t,\infty}}\right)}} \tag{42}$$

which is an expression relating the mass flow parameter m^* to the recovery factor r. An expression relating $\frac{\Delta\theta_{ss'}}{c}$ to r is also possible, but has not been derived here because $\frac{\Delta\theta_{ss'}}{c}$ is only a secondary variable.

Effect of Ducting Pressure Losses

In the actual application of a bleed air injection system there is a strong probability that ducting pressure losses will be incurred above and beyond those encountered in the normal manner of ejecting engine bleed or cabin air. These ducting pressure losses will reduce the velocity (but not mass flow if the proper adjustments are made to the slot width) and, hence, flow momentum at the slot exit. The reduced flow momentum represents an increment in drag that counteracts the favorable effects of low-energy air injection on skin friction. In equation form this increment in drag can be expressed as

$$\Delta C_{D_d} = \frac{\rho_e u_e w \left(u_e - u_{e,d}\right)}{q_\infty c} \tag{43}$$

where u_e is the exit velocity without ducting losses and $u_{e,d}$ is the exit velocity with ducting losses included. With the use of equation (14) the drag increment is converted to

$$\Delta C_{D_d} = 2\,\frac{m_e}{m_\infty}\left(\frac{u_e}{u_\infty} - \frac{u_{e,d}}{u_\infty}\right) \tag{44}$$

With the use of equations (15), (17), and (23), equation (44) is transformed into

$$\Delta C_{D_d} = 2\left[\left(\frac{\Delta\theta_{ss'}}{c}\right)_d - \frac{\Delta\theta_{ss'}}{c}\right] \tag{45}$$

or, the usually more convenient form

$$\Delta C_{D_d} = 2\,\frac{m_e}{m_\infty}\left(\frac{\theta_d{}^*}{m_d{}^*} - \frac{\theta^*}{m^*}\right) \tag{46}$$

At the same time that ducting pressure losses reduce slot exit velocities and momentum they will also have an effect on $\frac{\Delta\theta_{ss'}}{c}$. This effect is readily included in the calculations by using $\left(\frac{\Delta\theta_{ss'}}{c}\right)_d$ in equations (5) and (11) instead of $\frac{\Delta\theta_{ss'}}{c}$. Thus, in the final form, with ducting pressure losses included, the overall reductions in drag (combined effects of reductions in skin friction and losses in exit momentum) can be expressed as (from eq. (11))

$$\frac{\Delta C_D}{C_{F_{lt}}} = \frac{1}{C_{F_{lt}}}\left[\overline{C_{F_{lt'}}}\left(1 + \frac{\overline{\Delta ls}}{c} + \frac{\overline{ss'}}{c}\right) - 2\left(\frac{\Delta\theta_{ss'}}{c}\right)\right]_d + \frac{\Delta C_{D_d}}{C_{F_{lt}}} - 1 \tag{47}$$

where the subscript on the bracket signifies that all quantities within the brackets are to be based on $\left(\frac{\Delta\theta_{ss'}}{c}\right)_d$. If equation (45) is substituted in equation (47) the result is

$$\frac{\Delta C_D}{C_{F_{lt}}} = \frac{1}{C_{F_{lt}}}\left[\overline{C_{F_{lt'}}}\left(1 + \frac{\overline{\Delta ls}}{c} + \frac{\overline{ss'}}{c}\right)\right]_d + \frac{2}{C_{F_{lt}}}\frac{\Delta\theta_{ss'}}{c} - 1 \tag{48}$$

where the quantities within the brackets are again based on $\left(\frac{\Delta\theta_{ss'}}{c}\right)_d$.

RESULTS AND DISCUSSION

Incremental Boundary-Layer Momentum Thickness Parameter

General characteristics.- Inspection of equation (24) indicates that the incremental boundary-layer momentum thickness parameter θ^* is solely a function of the three variables m^*, M_∞, and $\frac{T_{t,e}}{T_{t,\infty}}$. Consequently, in figures 2 to 8 are presented some typical plots of the incremental boundary-layer momentum thickness parameter θ^* as a function of the injection-air mass-flow parameter m^* for various values of M_∞ and $\frac{T_{t,e}}{T_{t,\infty}}$. Figures 2 to 6 are intended primarily to show the connection of the two parameters θ^* and m^* with the pressure recovery factors r that are required to establish these flow characteristics in the absence of any auxiliary devices such as compressors or flow throttles. Figures 7 and 8 were prepared to show a clearer and more comprehensive picture of the general situation and to stress the effects of M_∞ and $\frac{T_{t,e}}{T_{t,\infty}}$.

Results indicate that, for $\frac{T_{t,e}}{T_{t,\infty}} = 1.0$ (figs. 2, 3, 4, and 7), θ^* is 0 when m^* is 0, increases to some maximum value, and then decreases to zero when $m^* = 1$. The physical interpretations are that there cannot be any increase in boundary-layer momentum thickness when there is no air injection and when the air is injected at stream velocity ($m^* = 1$). From the definition of θ^* in equation (23)

$$\theta^* = \frac{\frac{\Delta\theta_{ss'}}{c}}{w/c} = \frac{\Delta\theta_{ss'}}{w}$$

it is apparent that there is a maximum value of boundary-layer momentum thickness increase $\Delta\theta_{ss'}$ that can be attained for a particular slot width at constant Mach number. This maximum occurs at

$$(m^*)_{\theta^*_{max}} = \frac{1}{2}\sqrt{\frac{1}{\left(\frac{T_{t,e}}{T_{t,\infty}}\right)\left[1 - \left(\frac{\gamma - 1}{2} M_\infty{}^2\right)^2\right]}} \tag{49}$$

For values of m^* below those for θ^*_{max}, the mass flows through the slot are too low for maximum efficiency, and for values of m^* above those for θ^*_{max} the injection velocities are too high.

The effects of increasing Mach number at $\frac{T_{t,e}}{T_{t,\infty}} = 1$ are to decrease θ^* and hence to tend to lower the efficiency of the low-energy air-injection scheme over the full range of the mass-flow parameter but with increasing degree at the higher values of m^*. (See fig. 7.) Consequently, θ^*_{max} occurs at lower values of m^* (a desirable trend) at the high values of M_∞. The Mach number effect of decreasing θ^* is attributable to the fact that at constant m^* the exit velocity ratio u_e/u_∞ must be increased to compensate for the decreased density of the injection air at the higher Mach numbers. Much more could be said about the general characteristics of θ^*_{max}, but in subsequent discussions the importance of this parameter is severely downgraded and these additional characteristics become of little or no practical significance.

Included in figure 7 is a curve demarking the zones between subsonic and supersonic injection or exit velocities. This boundary is found by substituting the recovery factor required for sonic injection velocity

$$(r)_{M_e=1} = \frac{\left(1 + \frac{\gamma - 1}{2}\right)^{\frac{\gamma}{\gamma-1}} - 1}{\left(1 + \frac{\gamma - 1}{2} M_\infty{}^2\right)^{\frac{\gamma}{\gamma-1}} - 1} \tag{50}$$

into equation (42) and by using the resulting value of $(m^*)_{M_e=1}$ in equation (24).

The boundary for sonic slot exit or injection velocity (fig. 7) indicates that as M_∞ increases subsonic exit velocities will be achieved at progressively lower values of the mass-flow parameter m^*. Above a Mach number of about 2.2, it is impossible to attain the maximum theoretical boundary-layer thickening $\left(\theta^*_{max}\right)$ with subsonic injection velocities.

The effects of changes in the injection-air temperature ratio $\frac{T_{t,e}}{T_{t,\infty}}$ on θ^* at $M_\infty = 3$ can be deduced from figures 3, 5, 6, and 8. A decrease in $\frac{T_{t,e}}{T_{t,\infty}}$ causes an increase in θ^*, the effect increasing in magnitude as m^* increases. Increases in $\frac{T_{t,e}}{T_{t,\infty}}$, on the other hand, which are usually more readily attainable than decreases, have reversed effects. Finally, decreases in $\frac{T_{t,e}}{T_{t,\infty}}$ induce the largest improvements in θ^* at the highest pressure recovery factors. (Compare figs. 3, 5, and 6.) Increases have their most detrimental effect in this recovery factor range. These trends derive directly from the fact that low-temperature air injected into a boundary layer of higher than average temperature at constant m^* will require lower exit-velocity ratios to counterbalance the increased injection-air densities.

<u>θ^* as a function of u_e/u_∞</u>.- In the design of injection slots, it is generally desirable to know the exit or injection velocity. Consequently, figures 9 and 10 have been prepared to illustrate θ^* as a function of u_e/u_∞ for the same general conditions of Mach number and injection-air temperature ratio as were shown in figures 7 and 8.

In general, the same conclusions inferred from figures 7 and 8 for the Mach number and temperature-ratio effects in terms of mass-flow ratios m^* are derived from figures 9 and 10 for the effects in terms of the injection-velocity ratio u_e/u_∞. In addition, however, figure 9 displays the fact that at $\frac{T_{t,e}}{T_{t,\infty}} = 1$ the optimum value of θ^* occurs at increasing values of u_e/u_∞ as contrasted with decreasing values of m^* (fig. 7), as M_∞ increases. This reversal is readily explained on the basis of the increased exit-velocity ratios required to compensate for the decreased densities and which override effects of the diminished mass-flow ratios.

At constant Mach number (fig. 10) a decrease in $\frac{T_{t,e}}{T_{t,\infty}}$ increases θ^* and moves θ^*_{max} to higher values of u_e/u_∞. Conversely, an increase in $\frac{T_{t,e}}{T_{t,\infty}}$ decreases θ^* and moves θ^*_{max} to lower values of u_e/u_∞. These trends are in agreement with the requisites that at constant u_e/u_∞ increases in exit-flow temperature ratios be counteracted by decreases in mass-flow ratios. As is to be expected from the effects of temperature on the speed of sound, an increase in $\frac{T_{t,e}}{T_{t,\infty}}$ causes sonic exit velocity to occur at higher values of the velocity ratio u_e/u_∞.

Pressure Recovery Factor

Up to this point the pressure recovery factor r has been brought into the discussion several times but only in a general manner. It appears desirable at this point to examine the role of r in somewhat more detail. Accordingly, r has been presented as a function of the parameter $m^*\sqrt{\frac{T_{t,e}}{T_{t,\infty}}}$ (derived from eq. (42)) in figure 11.

The results of figure 11 indicate that r decreases rapidly with a decrease in the parameter $m^*\sqrt{\frac{T_{t,e}}{T_{t,\infty}}}$. The rate of decrease is largest for the highest Mach numbers. Probably the most noteworthy feature of this plot is the fact that very low recovery factors must be utilized to obtain the lower injection mass-flow ratios, particularly at the higher values of M_∞. This trend results from the fact that as the pressure differential between bleed-air inlet and exit is reduced to establish the smaller mass-flow ratios, the conversion of free-stream kinetic energy to heat decreases the density of the exit flow and tends to increase u_e/u_∞, and thus requires a still further decrease in the pressure differential to attain the desired m^*. This effect increases rapidly in potency as M_∞ increases owing to the sharp rise in stagnation pressures.

Reductions in Skin-Friction Parameter

The ultimate objective of this investigation was to determine the possible reductions in the skin-friction parameter $\frac{\Delta C_F}{C_{F_{lt}}}$ as a function of the pressure recovery factor r. Such an approach insures the compatibility of the variables involved and limits the analysis to physical flows attainable without the use of throttles or some type of pump. Results of the theoretical calculations are presented in two ways. In figures 12 to 18, $\frac{\Delta C_F}{C_{F_{lt}}}$ is presented as a function of r, each one of the significant variables being used as a parameter while the others are being held constant. In figures 19 to 25 $\frac{\Delta C_F}{C_{F_{lt}}}$ is presented as a function of each one of the variables, the others being held constant but with r always as the varying parameter.

The results of figures 12 to 25 indicate that the greatest reductions in skin friction are obtained always at the lowest recovery factors and that the rate of reduction generally strongly increases as r decreases. This result means that the greatest reductions in skin friction will be obtained with the lowest possible injection velocities and widest slots and that θ^*_{max} is not a parameter of any great significance. At a supersonic Mach number of 3, for the limited range of parameters studied in this investigation, the largest reduction in $\frac{\Delta C_F}{C_{F_{lt}}}$ that was calculated was on the order of 0.24 (or 24 percent) and this value occurred for a slot located at 5 percent of the chord $\left(\frac{l_s}{c} = 0.05\right)$, for a mass-flow ratio of 0.002 and for a recovery factor of only 0.005 (fig. 15). For a more reasonable and anticipated bleed-air pressure-recovery range of 0.25 to 0.50, the reduction in skin friction is on the order of 10 to 5 percent (figs. 15 and 22). For an application restricted to reduction of skin friction on an engine nacelle only the mass-flow ratios can be higher than those investigated herein, and the theoretical nacelle skin-friction reductions may be higher than those quoted previously.

The effects of increasing M_∞ at constant r are to reduce $\frac{\Delta C_F}{C_{F_{lt}}}$ sharply in the range of recovery factors that probably will be encountered in actual service. (See figs. 12 and 19.) This trend derives from the aforementioned fact that conversion of free-stream kinetic energy into heat in the pressure-loss phase of the bleed-air flow will decrease the density of the injected air and require higher injection velocities at constant mass flow, which in turn will increase the momentum of the injected air and hence lower the efficiency of this air-injection scheme.

Increasing R_∞ decreases the value of $\frac{\Delta C_F}{C_{F_{lt}}}$ slightly. (See figs. 13 and 20.) It may be noted that the Reynolds numbers were chosen to correspond to those for a wing having an average chord of 35 feet, such as might be of interest for a supersonic transport operating at unit Reynolds numbers of 0.5, 1.5, 3.0, and 5.0.

Changes in injection-air temperature ratio have a powerful effect on the skin-friction reduction (figs. 14 and 21) and lead to consideration of spent cabin air (which is apt to be relatively cool) for injection if sufficient quantities of such air are available. The physical basis for the effects of changes in $\frac{T_{t,e}}{T_{t,t}}$ on the momentum thickness parameter θ^*, which is the main variable involved in producing the trends, has been discussed previously.

Installation of the injection slot as close to the leading edge as possible is important for skin-friction reduction (figs. 15 and 22) although such an installation may often lead to structural and wave-drag problems which may tend to counteract the favorable effect of air injection.

Increasing the chord length has a small favorable effect on reduction in skin-friction parameter (figs. 16 and 23), but it should be noted that this comparison involves a change in injection-air mass flow (even though the mass-flow ratio m_e/m_∞ is constant). Increasing the chord at constant absolute mass flow (figs. 17 and 24) generally results in large decreases in $\frac{\Delta C_F}{C_{F_{lt}}}$ as expected.

Finally, but most significantly, decreases in the mass-flow ratio m_e/m_∞ lead to substantial decreases in the possible reductions in skin friction. (See figs. 18 and 25.) A reduction of m_e/m_∞ to 0.001 will provide reductions in skin friction only on the order of 6 to 2 percent for the pressure recovery factor range of 0.25 to 0.50 even for the most forward slot location (data not shown) at Mach number 3. This mass-flow ratio is probably a substantially more realistic value of available engine bleed air than the value of 0.002 used in most of the calculations if air injection is to be applied to a complete wing. On the other hand, if air injection is restricted to an engine nacelle the mass-flow ratios can be higher than those considered herein, and the reductions in nacelle skin friction may be higher than those quoted for the largest values of m_e/m_∞ investigated. There would be no improvement, however, in terms of complete airplane drag.

Effects of Ducting Pressure Losses

The effects of ducting pressure losses on the drag reduction parameter $\frac{\Delta C_D}{C_{F_{lt}}}$ (where the momentum in the engine bleed-air flow at the injection slot is assumed to be fully recoverable) have been calculated for a few specific cases and the results are presented in figures 26 to 32. In these figures the dashed line represents the reduction in drag that is possible without ducting losses and the solid line represents the reduction in drag that is obtained with ducting losses.

The solid lines in these figures are interpreted as follows: If the pressure recovery factor for a specific set of conditions (fig. 30) is 0.455 and the slot width is 0.00230, then the value of $\frac{\Delta C_D}{C_{F_{lt}}}$ for no ducting losses is slightly more than -0.08 $\left(\text{and } \frac{\Delta C_D}{C_{F_{lt}}} = \frac{\Delta C_F}{C_{F_{lt}}}\right)$. If there are ducting pressure losses, then the same mass flow through the injection slot can be maintained only by increasing the recovery factor of the bleed air by the amount of the pressure losses. The resultant loss in momentum in the bleed-air flow counteracts the favorable effects of the reductions in skin friction and the overall reduction in drag represented by the increment in drag parameter $\frac{\Delta C_D}{C_{F_{lt}}}$ is decreased. Thus, at $r = 0.60$ the ducting pressure losses are found to be equal to an increment in r of -0.145 and the value of $\frac{\Delta C_D}{C_{F_{lt}}}$ is only about -0.015 or -1.5 percent. If r had been 0.60 and there were no ducting pressure losses, then $\frac{\Delta C_D}{C_{F_{lt}}}$ would have been about -0.075. The decrease in $\frac{\Delta C_D}{C_{F_{lt}}}$ from -0.075 to -0.015 at $r = 0.60$ represents the loss in overall drag reduction resulting from the introduction of the ducting losses at constant bleed-air pressure recovery factor.

Examination of figures 26 to 32 indicates that ducting pressure losses rapidly decrease the effectiveness of the scheme of reducing turbulent skin friction by low-energy air injection. This is particularly true at the low recovery factors where the effectiveness of air injection is greatest. For $\frac{T_{t,e}}{T_{t,\infty}} = 1.0$, ducting pressure recovery losses Δr of less than 0.1 will negate all possible favorable effects of reduction in skin friction in the range of r near 0.5. For r near 0.1, the ducting losses need be less than 0.05 to have the same adverse effect. Thus, it appears that skin-friction reduction by low-energy air injection will be practical only where ducting requirements will be minimum, such as on an engine nacelle with the use of engine bleed air and on a fuselage with spent cabin air. It may even be possible that in some such air-injection installations, the internal ducting losses suffered in ejecting bleed or cabin air actually may be reduced and a double dividend obtained.

Further inspection of figures 26 to 32 reveals no significant changes in trends due to Mach number effects (compare figs. 26, 27, and 28), due to R_∞ effects (compare figs. 27 and 29), due to changes in air-injection temperature ratio $\frac{T_{t,e}}{T_{t,\infty}}$ (compare figs. 27 and 30), due to slot location (compare figs. 27

and 31), or due to reductions in mass-flow ratio m_e/m_∞ (compare figs. 27 and 32). Another factor to note is that the slot-width to chord ratios w/c coupled with the expected range of bypass recovery factors (0.25 to 0.50) will be small, generally less than 0.004. For the lowest recovery factor of 0.01 the associated slot-chord ratios are on the order of 0.01 to 0.02.

Comparison of Theory With Experiment

A limited comparison has been made of the theoretical indications with some unpublished air-injection results obtained on a semispan wing by means of force tests at a Mach number of 2 and with some results obtained by momentum surveys on a flat plate at a Mach number of 3 from reference 9. The force data appear to confirm the general indications of the theory whereas the results of the momentum investigation appear to be in disagreement. More experimental information is needed, however, before a final assessment of agreement of theory with experiment is justified.

SUMMARY OF RESULTS

An analytical investigation based on a number of simplifying assumptions has been made of the possibilities of reduction in compressible turbulent skin friction on a flat plate by means of low-energy air injection through discrete slots. The analysis is based on the combination of the momentum losses in the boundary-layer and injection-air flows, and employs the Sommer and Short reference temperature method for estimating boundary-layer skin friction. The results of the analysis indicate

1. The greatest theoretical reductions in skin friction occurred at the lowest injection-air pressure recovery factors defined as the fraction of free-stream dynamic pressure energy still preserved in the injection or engine bleed air after entrance losses, and thus at the lowest air injection velocities.

2. For the optimum set of conditions considered in the analysis, the maximum reduction in skin friction at a Mach number of 3 was about 24 percent at a recovery factor of 0.005. For an anticipated pressure recovery range of 0.25 to 0.50, the calculated reduction in skin friction with the remaining conditions being held constant was on the order of 10 to 5 percent.

3. In general, increases in free-stream Mach number, increases in free-stream Reynolds number per foot, internal heating of the bleed air, and movement of the injection slot downstream from the leading edge led to decreases in the available reductions in skin friction; whereas, internal cooling of the bleed air, increases in chord length at constant injection mass flow, and increases in injection-air mass flow resulted in increases in the amount of reduction in skin friction that is possible.

4. Pressure losses in injection-air ducting rapidly negated the favorable effects of air injection.

Langley Research Center,
National Aeronautics and Space Administration,
Langley Station, Hampton, Va., August 4, 1964.

REFERENCES

1. Dorrance, William H., and Dore, Frank J.: The Effect of Mass Transfer on the Compressible Turbulent Boundary-Layer Skin Friction and Heat Transfer. Jour. Aero. Sci., vol. 21, no. 6, June 1954, pp. 404-410.

2. Rubesin, Morris W.: An Analytical Estimation of the Effect of Transpiration Cooling on the Heat-Transfer and Skin-Friction Characteristics of a Compressible, Turbulent Boundary Layer. NACA TN 3341, 1954.

3. Clarke, Joseph H., Menkes, Hans R., and Libby, Paul A.: A Provisional Analysis of Turbulent Boundary Layers With Injection. Jour. Aero. Sci., vol. 22, no. 4, Apr. 1955, pp. 255-260.

4. Persh, Jerome: A Theoretical Investigation of the Effect of Injection of Air on Turbulent Boundary-Layer Skin-Friction and Heat-Transfer Coefficients at Supersonic and Hypersonic Speeds. NAVORD Rep. 4220, U.S. Naval Ord. Lab. (White Oak, Md.), Jan. 4, 1957.

5. Tendeland, Thorval, and Okuno, Arthur F.: The Effect of Fluid Injection on the Compressible Turbulent Boundary Layer - The Effect on Skin Friction of Air Injected Into the Boundary Layer of a Cone at $M = 2.7$. NACA RM A56D05, 1956.

6. Sommer, Simon C., and Short, Barbara J.: Free-Flight Measurements of Turbulent-Boundary-Layer Skin Friction in the Presence of Severe Aerodynamic Heating at Mach Numbers From 2.8 to 7.0. NACA TN 3391, 1955.

7. Peterson, John B., Jr.: A Comparison of Experimental and Theoretical Results for the Compressible Turbulent-Boundary-Layer Skin Friction With Zero Pressure Gradient. NASA TN D-1795, 1963.

8. Bradfield, Walter S.: An Experimental Investigation of the Turbulent Boundary Layer in Supersonic Flow Around Unyawed Cones With Small Heat Transfer and Correlations With Two Dimensional Data. Res. Rep. No. 1, Convair Sci. Res. Lab., Mar. 15, 1958.

9. McRee, Donald I., Peterson, John B., Jr., and Braslow, Albert L.: Effect of Air Injection Through a Porous Surface and Through Slots on Turbulent Skin Friction at Mach 3. NASA TN D-2427, 1964.

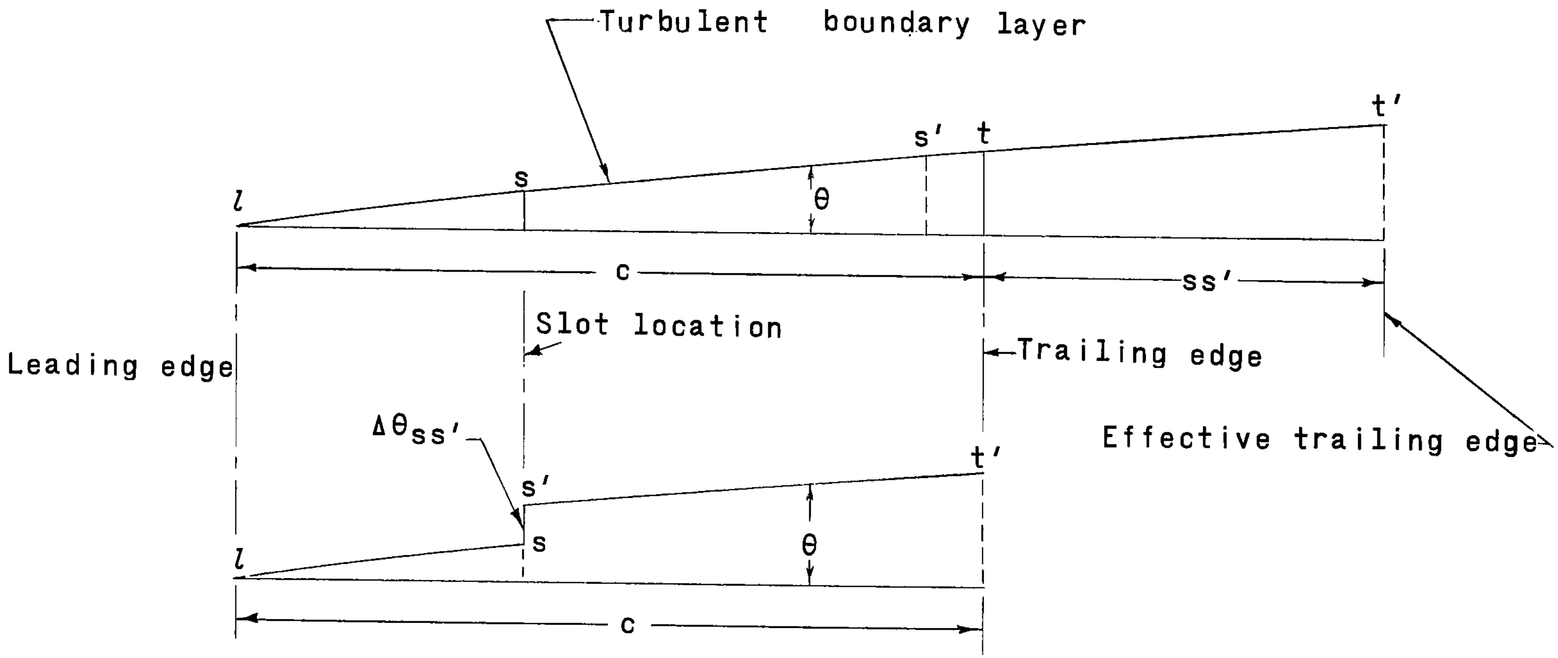

Figure 1.- Assumed boundary-layer model for analytical investigation.

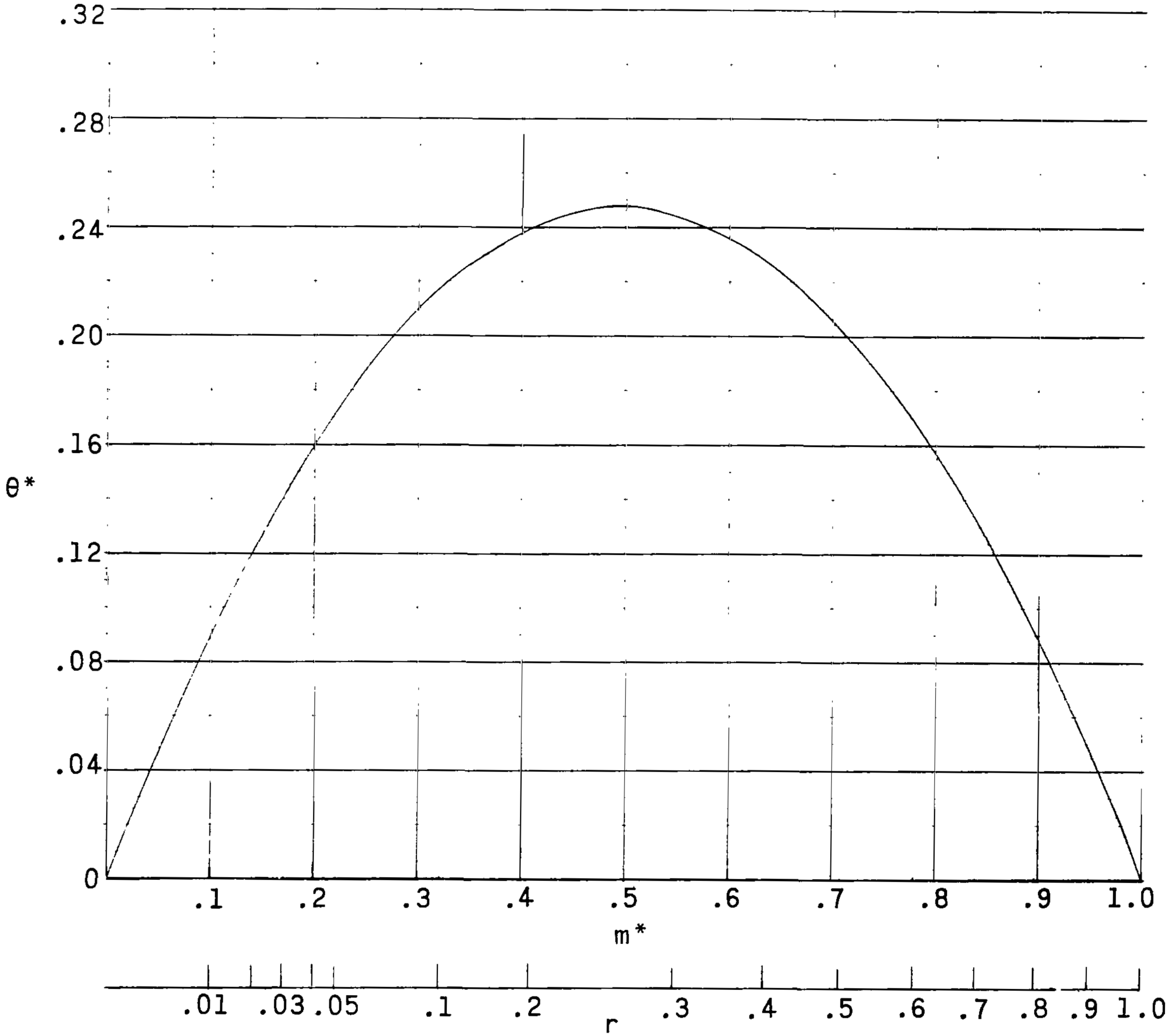

Figure 2.- Variation of θ^* with m^* and r. $M_\infty = 0.1$; $\frac{T_{t,e}}{T_{t,\infty}} = 1.0$.

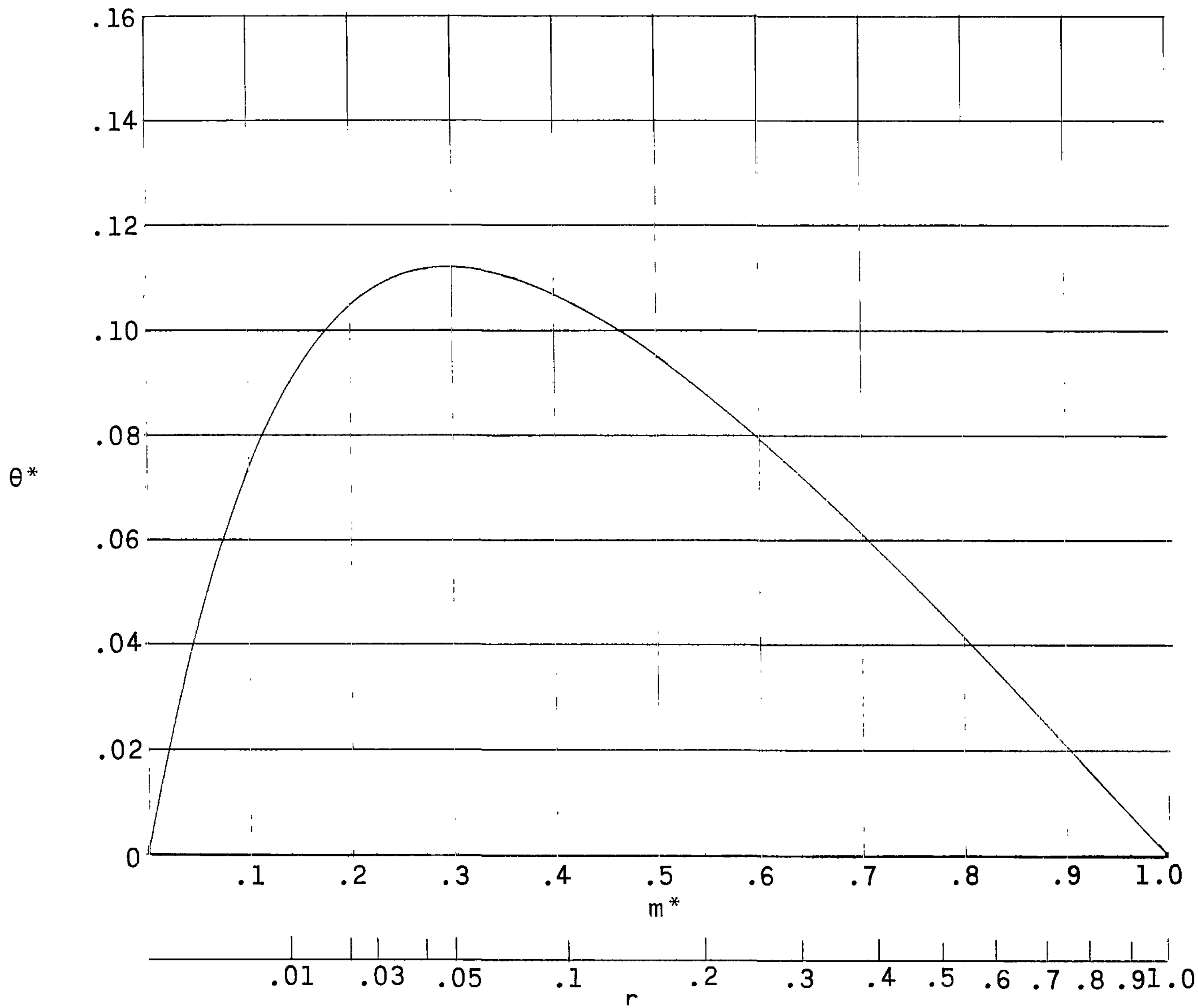

Figure 3.- Variation of θ^* with m^* and r. $M_\infty = 3.0$; $\frac{T_{t,e}}{T_{t,\infty}} = 1.0$.

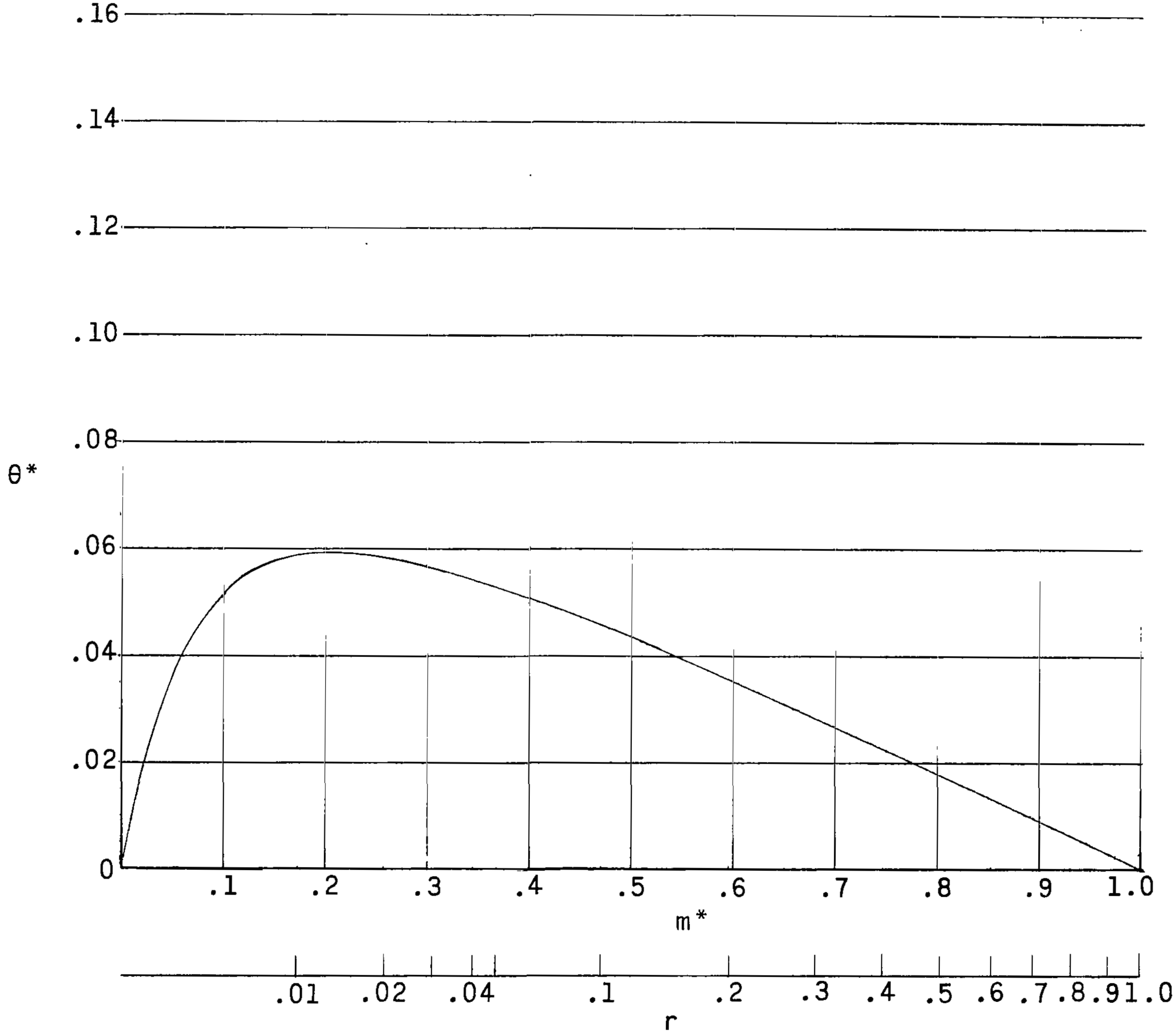

Figure 4.- Variation of θ^* with m^* and r. $M_\infty = 5.0$; $\dfrac{T_{t,e}}{T_{t,\infty}} = 1.0$.

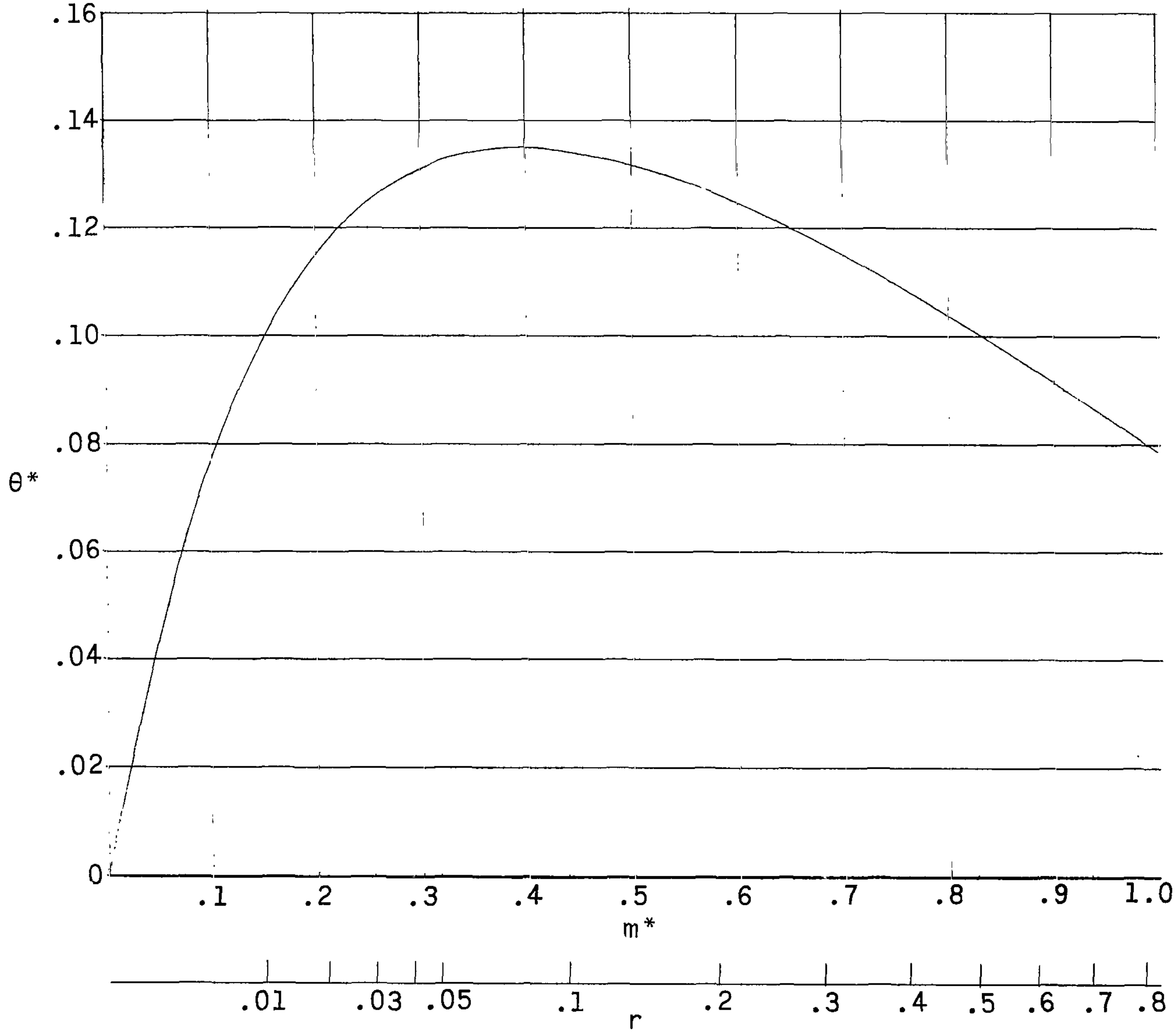

Figure 5.- Variation of θ^* with m^* and r. $M_\infty = 3.0$; $\frac{T_{t,e}}{T_{t,\infty}} = 0.875$.

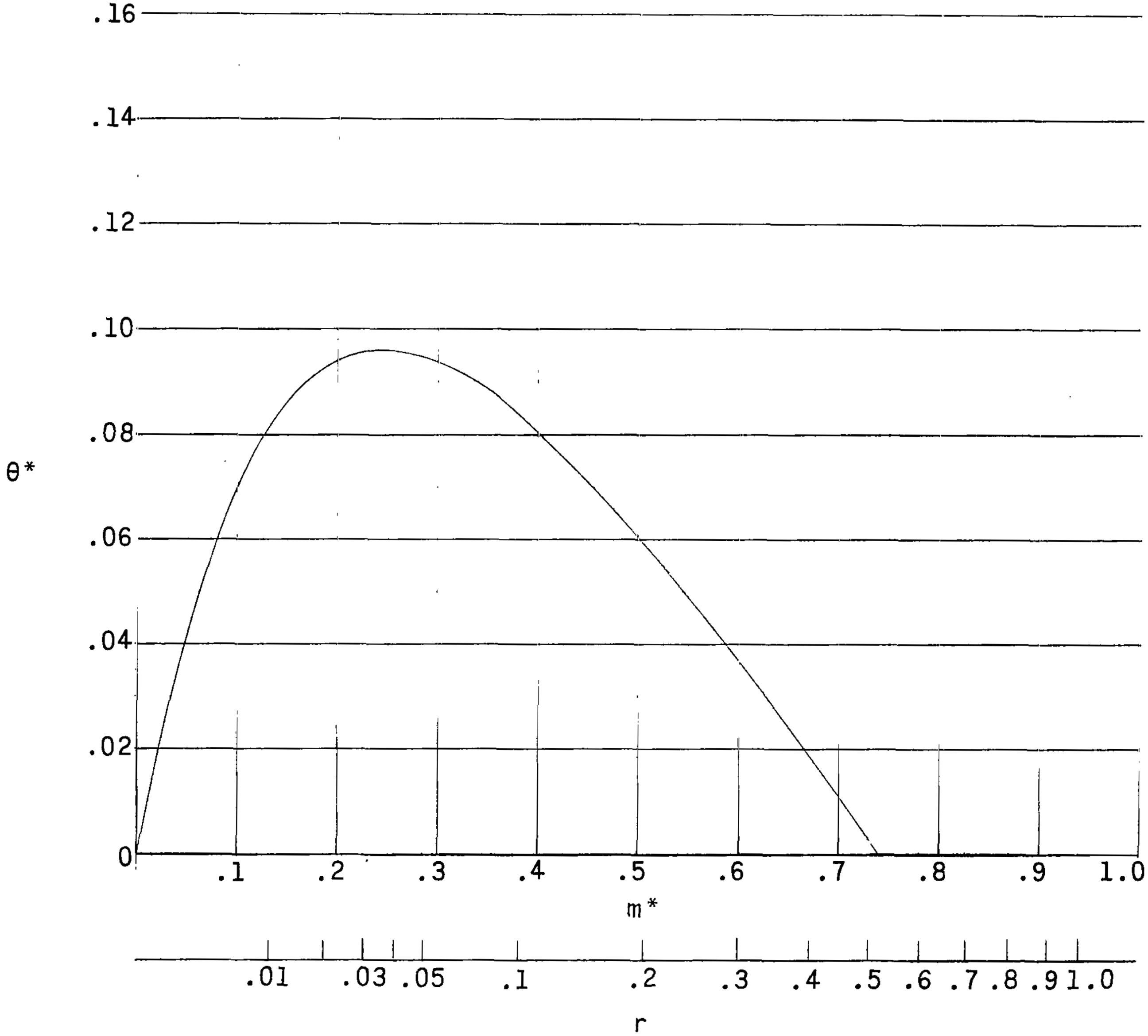

Figure 6.- Variation of θ^* with m^* and r. $M_\infty = 3.0$; $\frac{T_{t,e}}{T_{t,\infty}} = 1.125$.

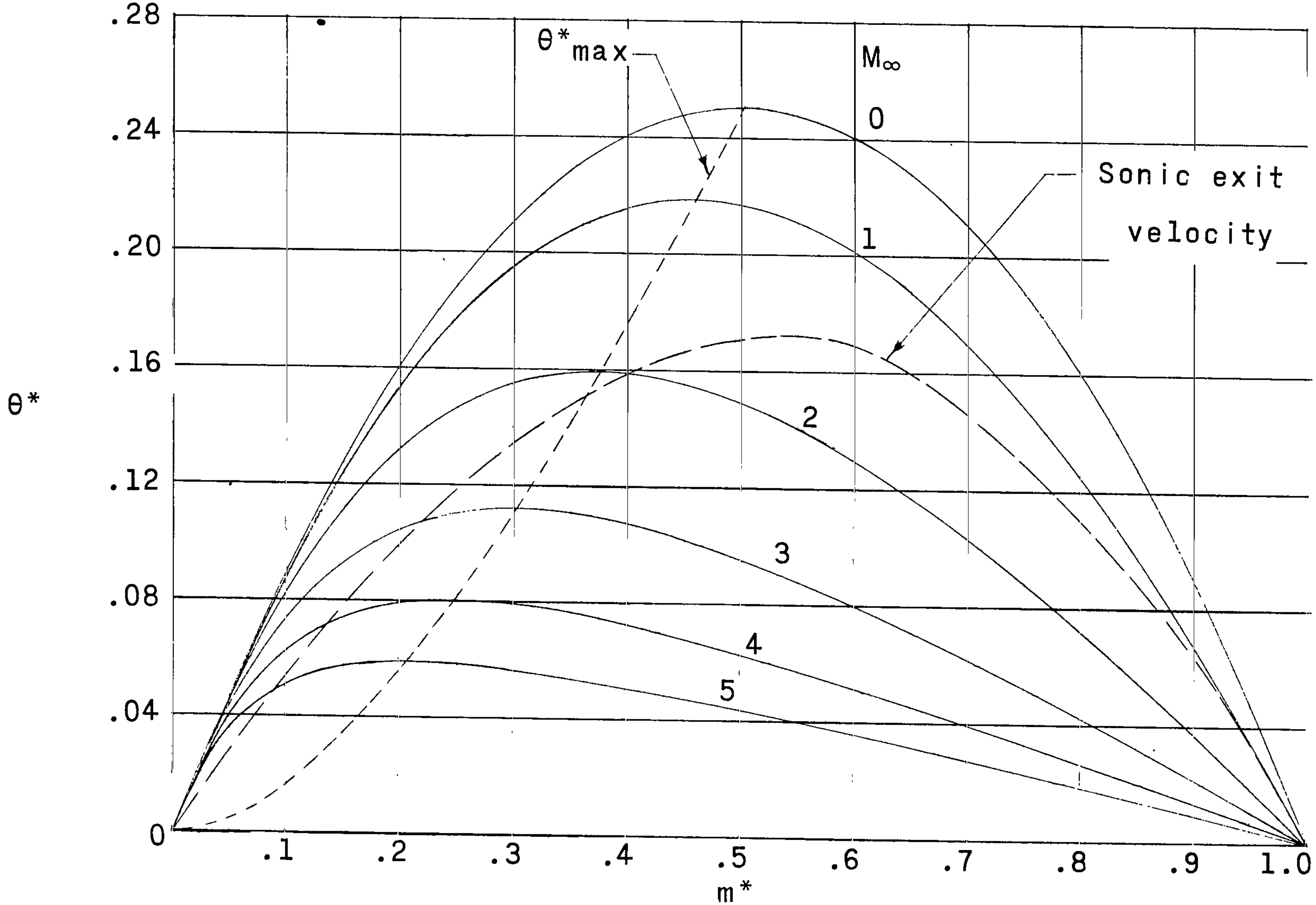

Figure 7.- Effect of M_∞ on variation of θ^* with m^*. $\frac{T_{t,e}}{T_{t,\infty}} = 1.0$.

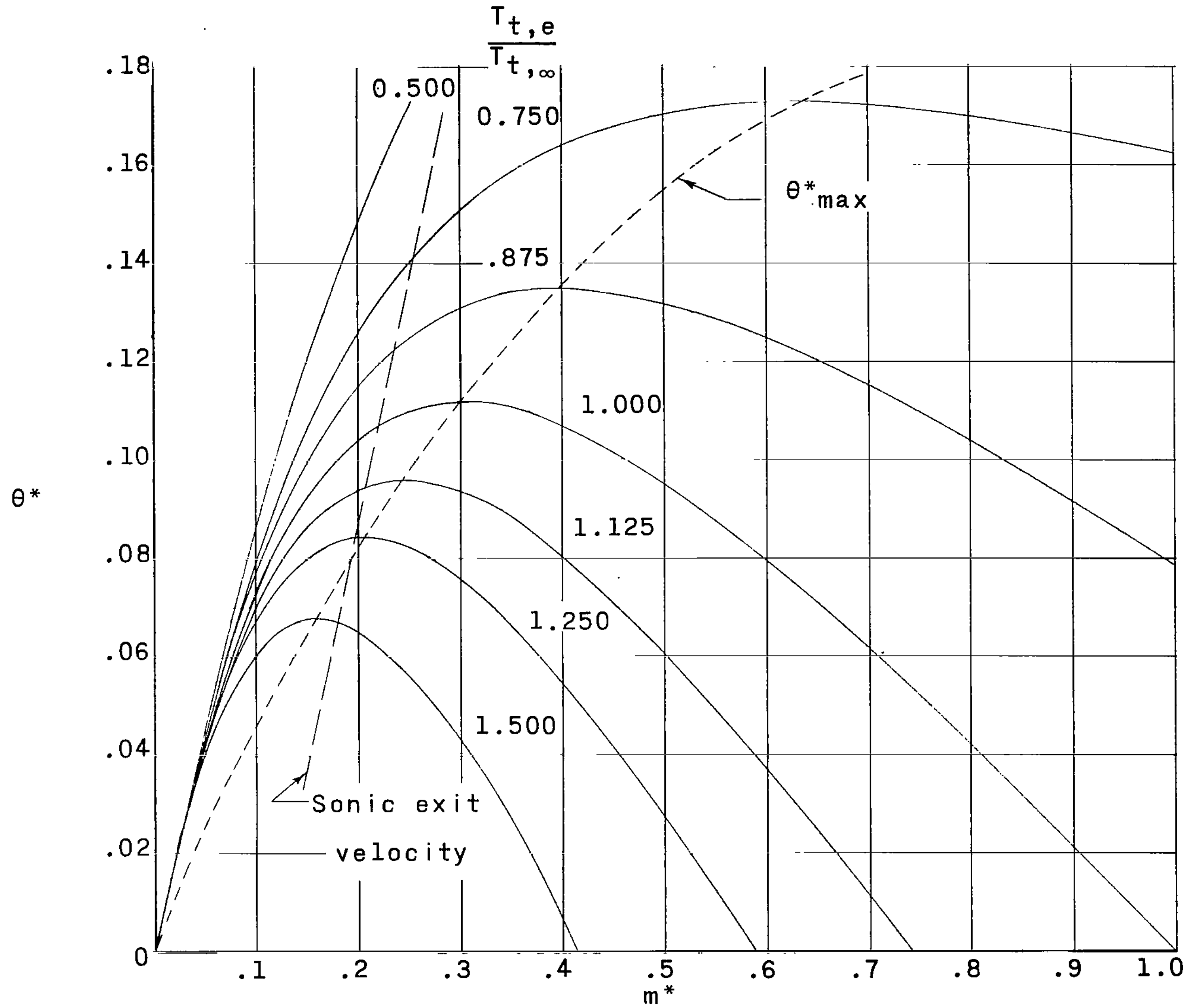

Figure 8.- Effect of $\frac{T_{t,e}}{T_{t,\infty}}$ on variation of θ^* with m^*. $M_\infty = 3.0$.

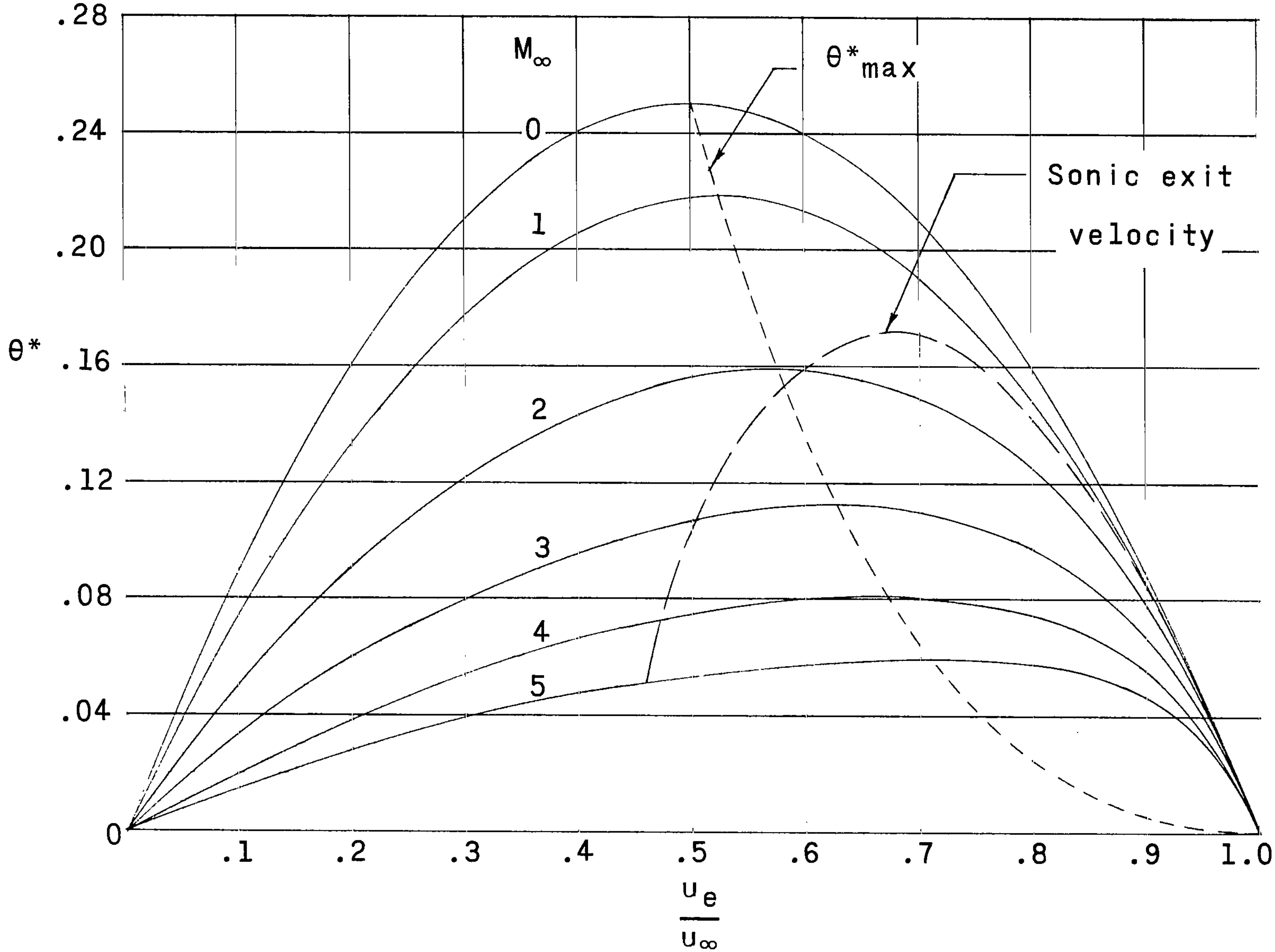

Figure 9.- Effect of M_∞ on variation of θ^* with $\frac{u_e}{u_\infty}$. $\frac{T_{t,e}}{T_{t,\infty}} = 1.0$.

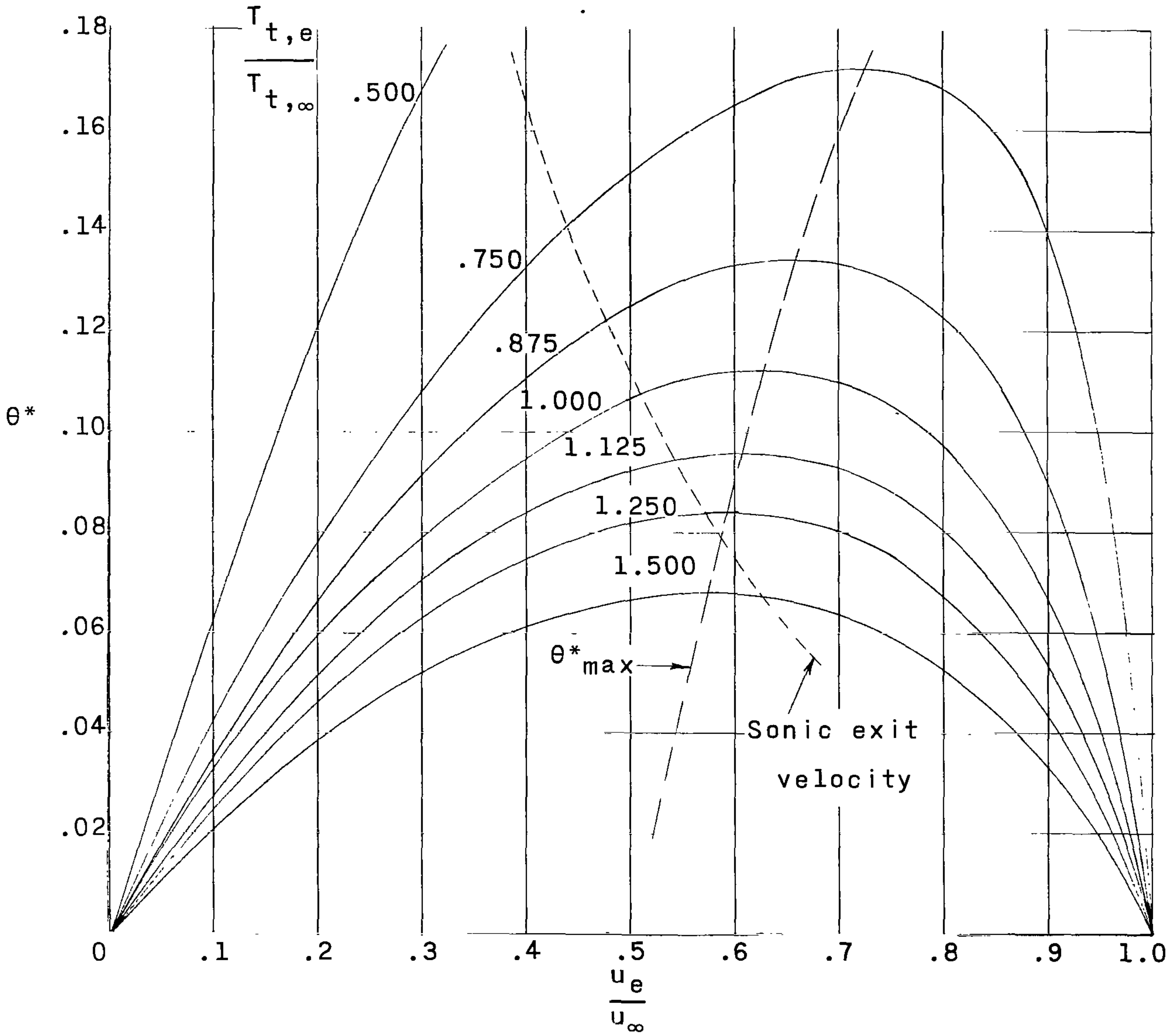

Figure 10.- Effect of $\frac{T_{t,e}}{T_{t,\infty}}$ on variation of θ^* with $\frac{u_e}{u_\infty}$. $M_\infty = 3.0$.

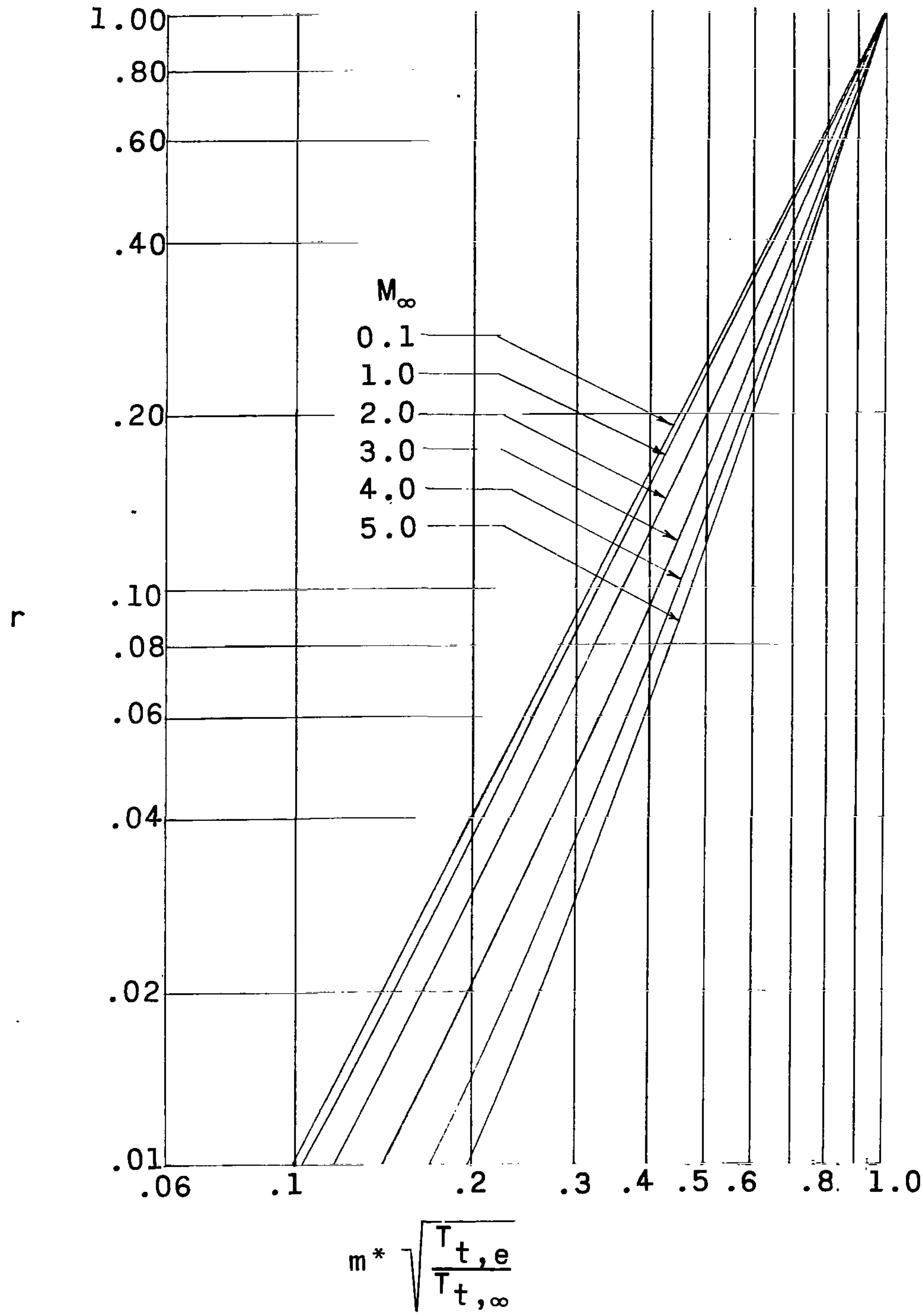

Figure 11.- Effect of M_∞ on parameter $m^*\sqrt{\frac{T_{t,e}}{T_{t,\infty}}}$.

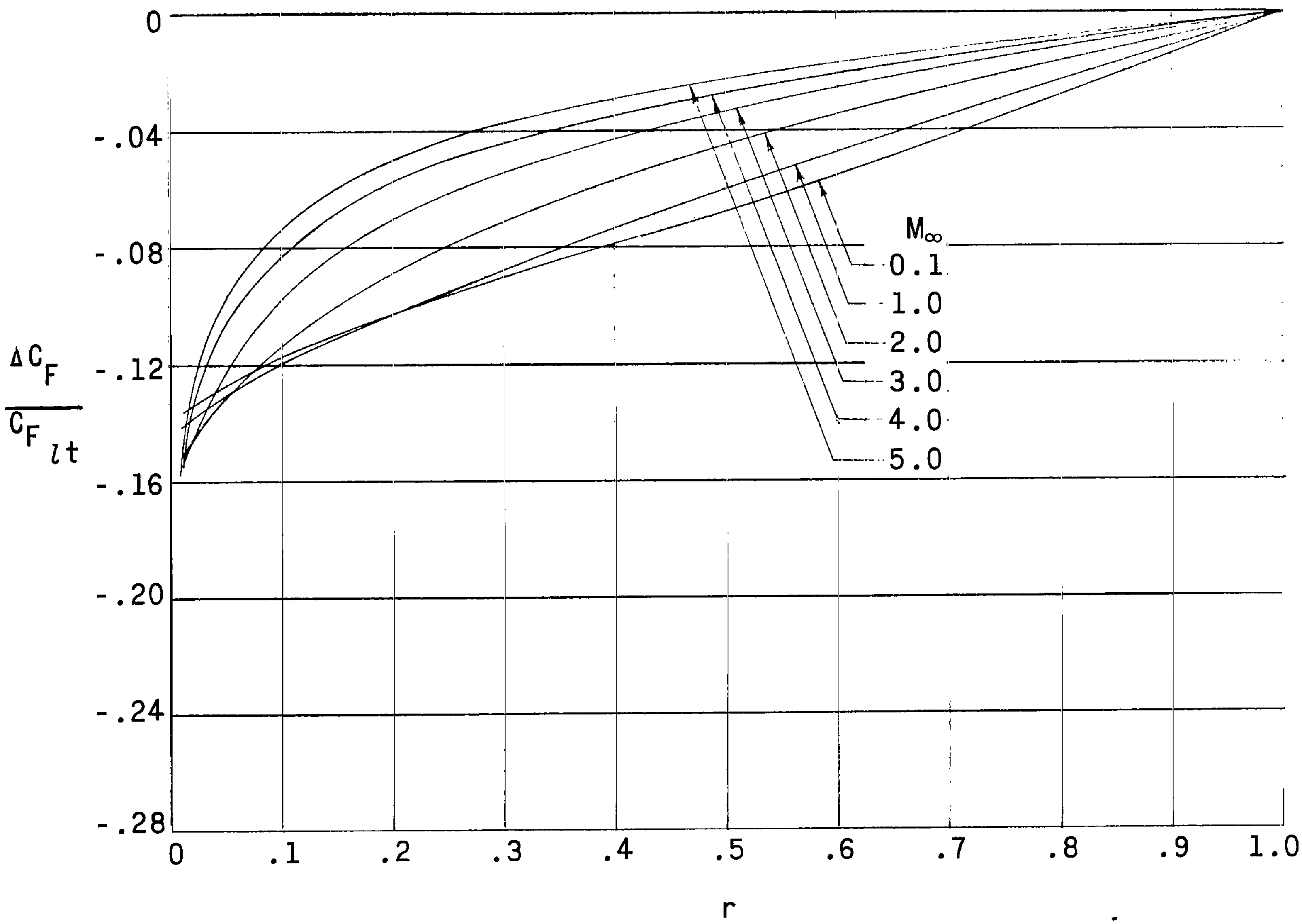

Figure 12.- Effect of M_∞ on variation of $\frac{\Delta C_F}{C_{F_{lt}}}$ with r. $R_\infty = 52.5 \times 10^6$; $\frac{T_{t,e}}{T_{t,\infty}} = 1.0$; $\frac{ls}{c} = 0.20$; $\frac{m_e}{m_\infty} = 0.002$.

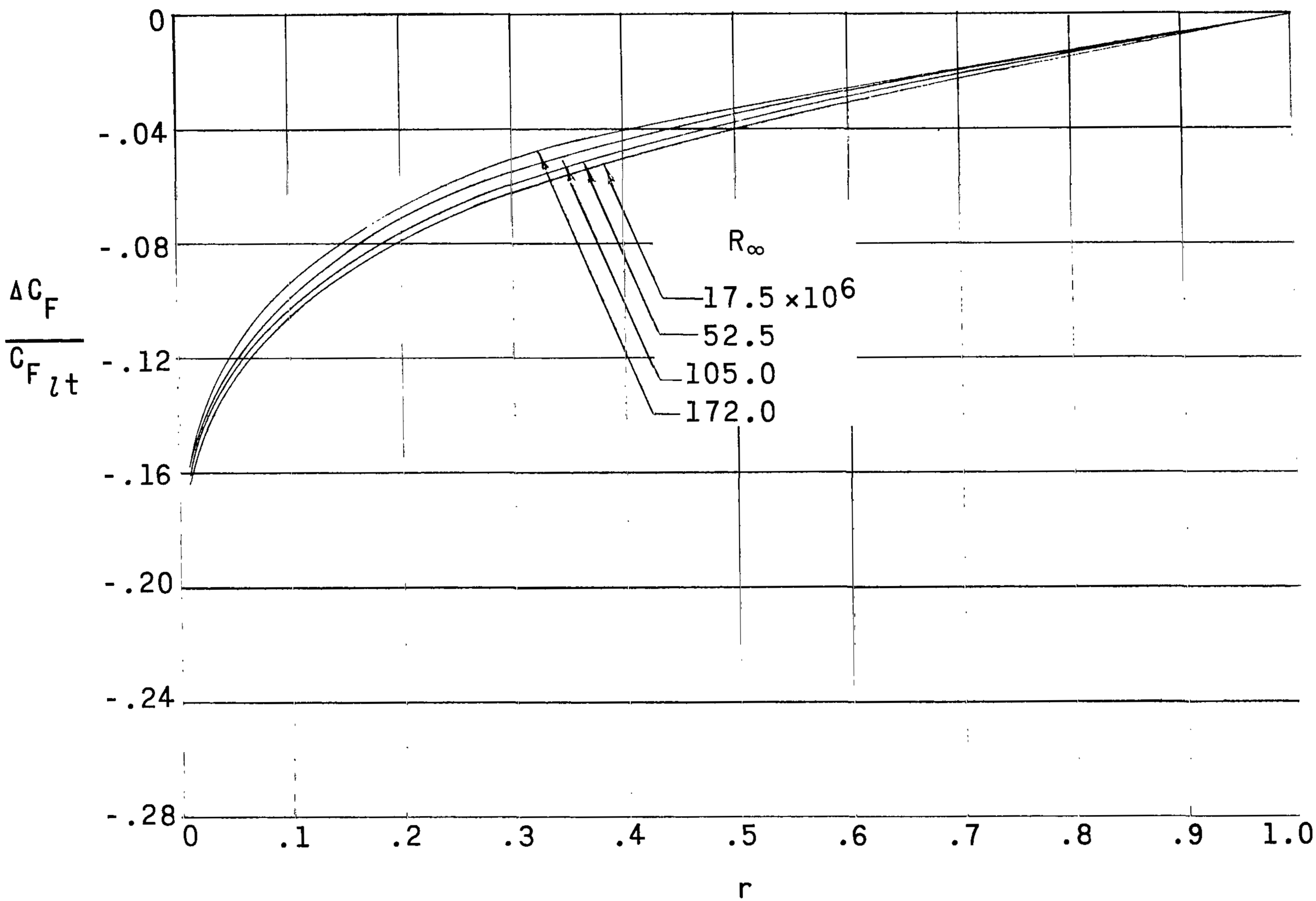

Figure 13.- Effect of R_∞ on variation of $\frac{\Delta C_F}{C_{F_{lt}}}$ with r. $M_\infty = 3.0$; $\frac{T_{t,e}}{T_{t,\infty}} = 1.0$; $\frac{ls}{c} = 0.20$; $\frac{m_e}{m_\infty} = 0.002$.

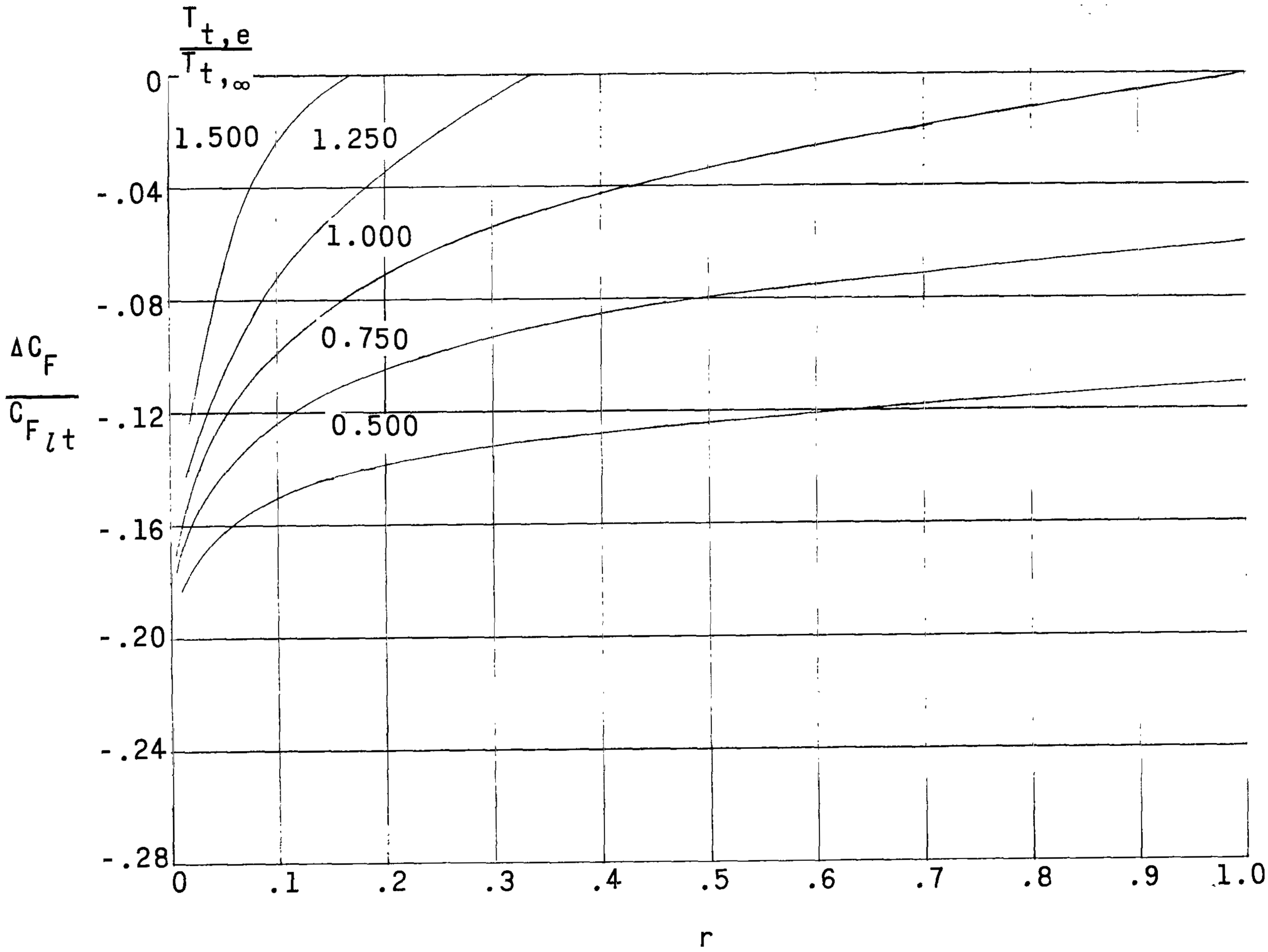

Figure 14.- Effect of $\frac{T_{t,e}}{T_{t,\infty}}$ on variation of $\frac{\Delta C_F}{C_{F_{lt}}}$ with r. $M_\infty = 3.0$; $R_\infty = 52.5 \times 10^6$; $\frac{ls}{c} = 0.20$; $\frac{m_e}{m_\infty} = 0.002$.

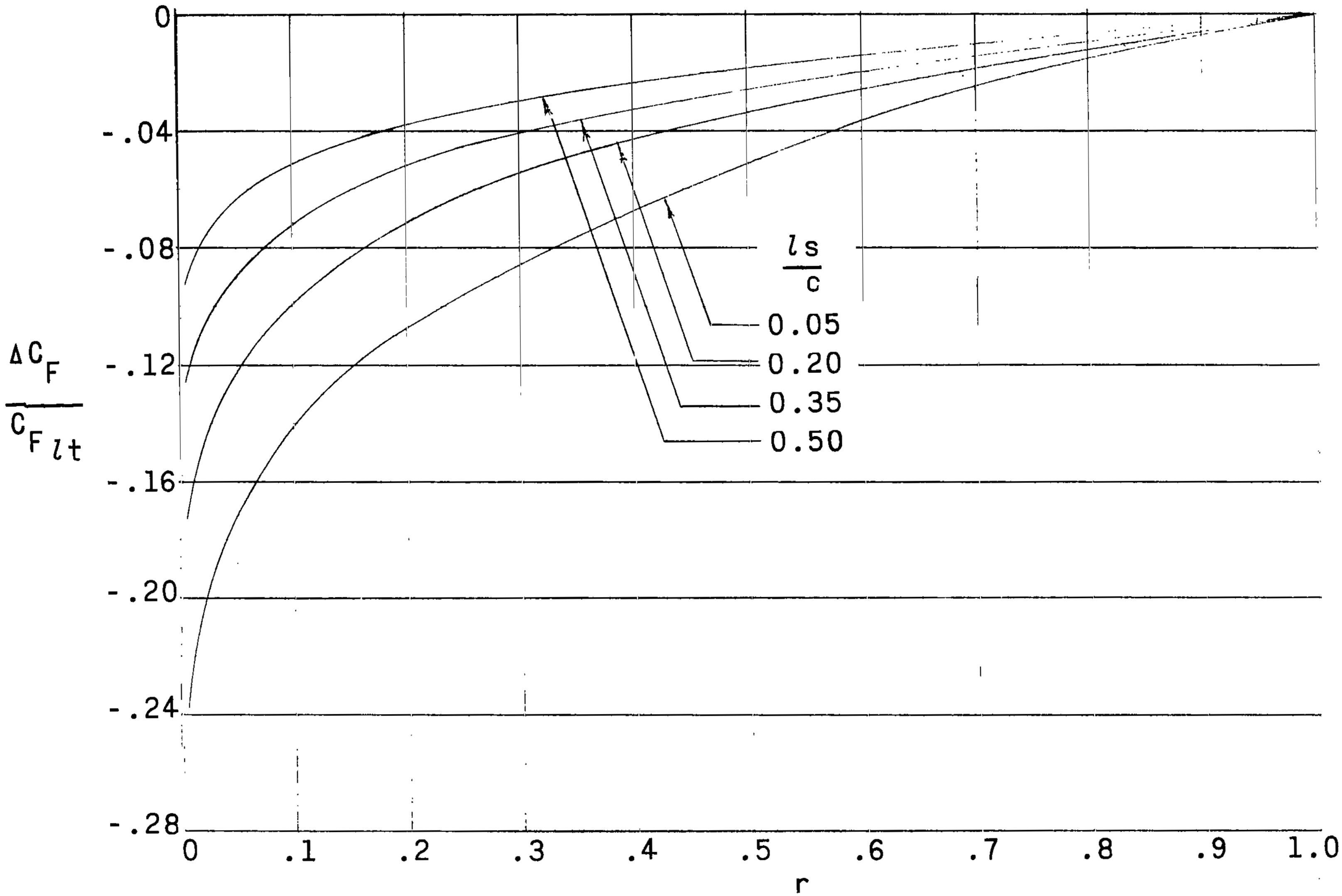

Figure 15.- Effect of $\frac{ls}{c}$ on variation of $\frac{\Delta C_F}{C_{F_{lt}}}$ with r. $M_\infty = 3.0$; $R_\infty = 52.5 \times 10^6$; $\frac{T_{t,e}}{T_{t,\infty}} = 1.0$; $\frac{m_e}{m_\infty} = 0.002$.

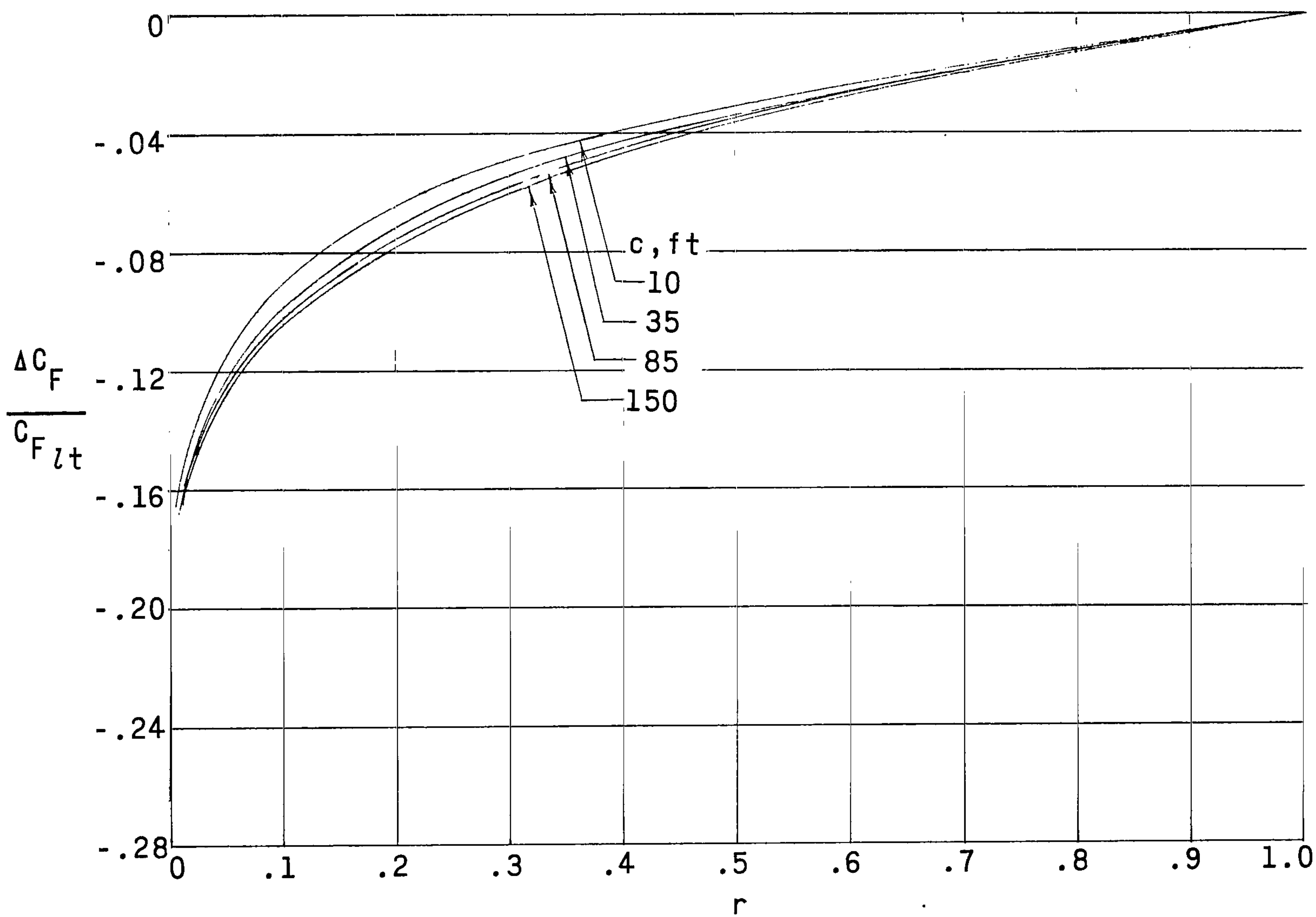

Figure 16.- Effect of c on variation of $\frac{\Delta C_F}{C_{F_{lt}}}$ with r at a constant $\frac{m_e}{m_\infty}$. $M_\infty = 3.0$; $R_{ft} = 1.5 \times 10^6$; $\frac{T_{t,e}}{T_{t,\infty}} = 1.0$; $\frac{ls}{c} = 0.20$; $\frac{m_e}{m_\infty} = 0.002$.

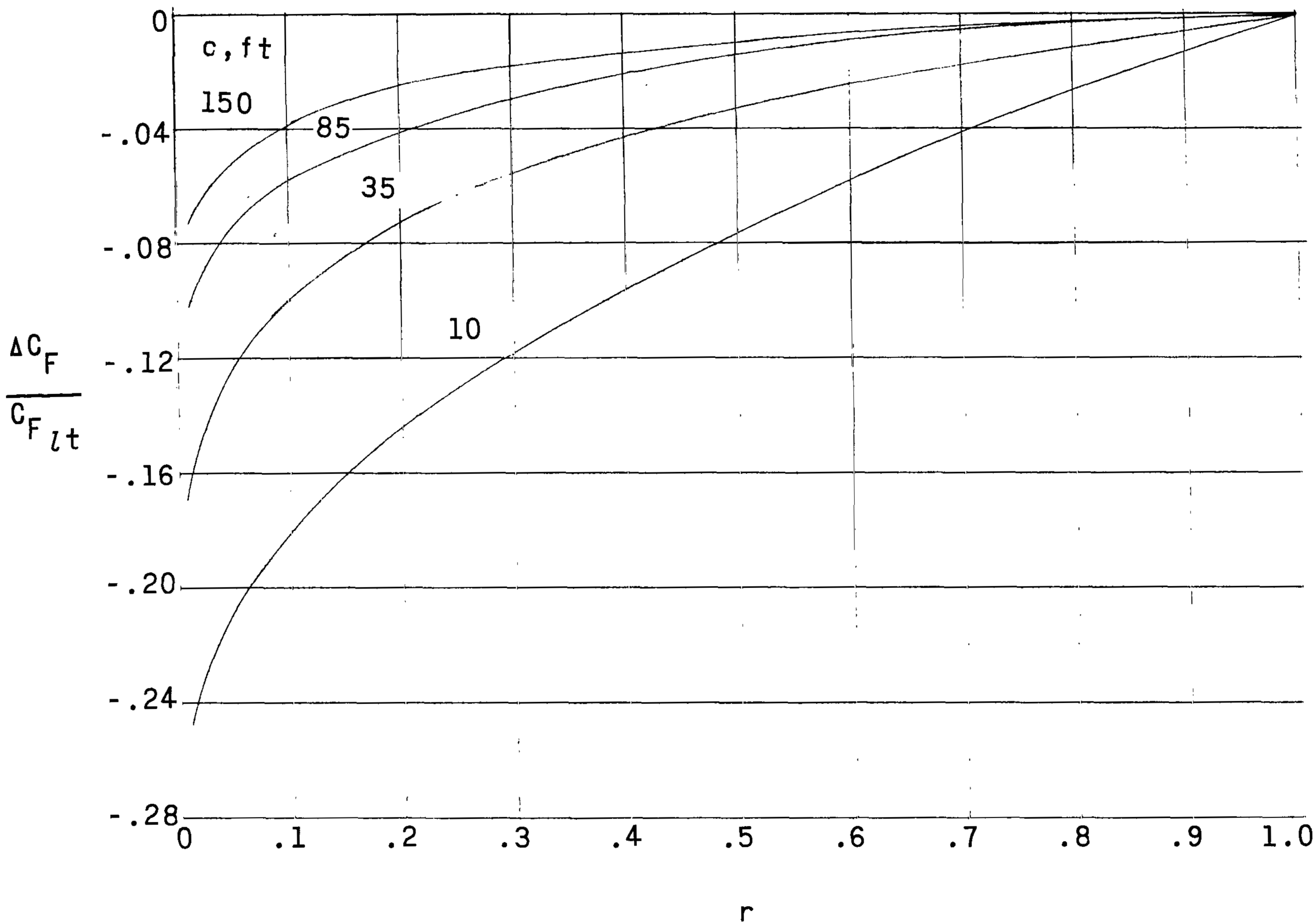

Figure 17.- Effect of c on variation of $\frac{\Delta C_F}{C_{F_{lt}}}$ with r at a constant $\frac{m_e}{m_\infty}\frac{c}{c_{35}}$. $M_\infty = 3.0$; $R_{ft} = 1.5 \times 10^6$; $\frac{T_{t,e}}{T_{t,\infty}} = 1.0$; $\frac{ls}{c} = 0.20$; $\frac{m_e}{m_\infty}\frac{c}{c_{35}} = 0.002$.

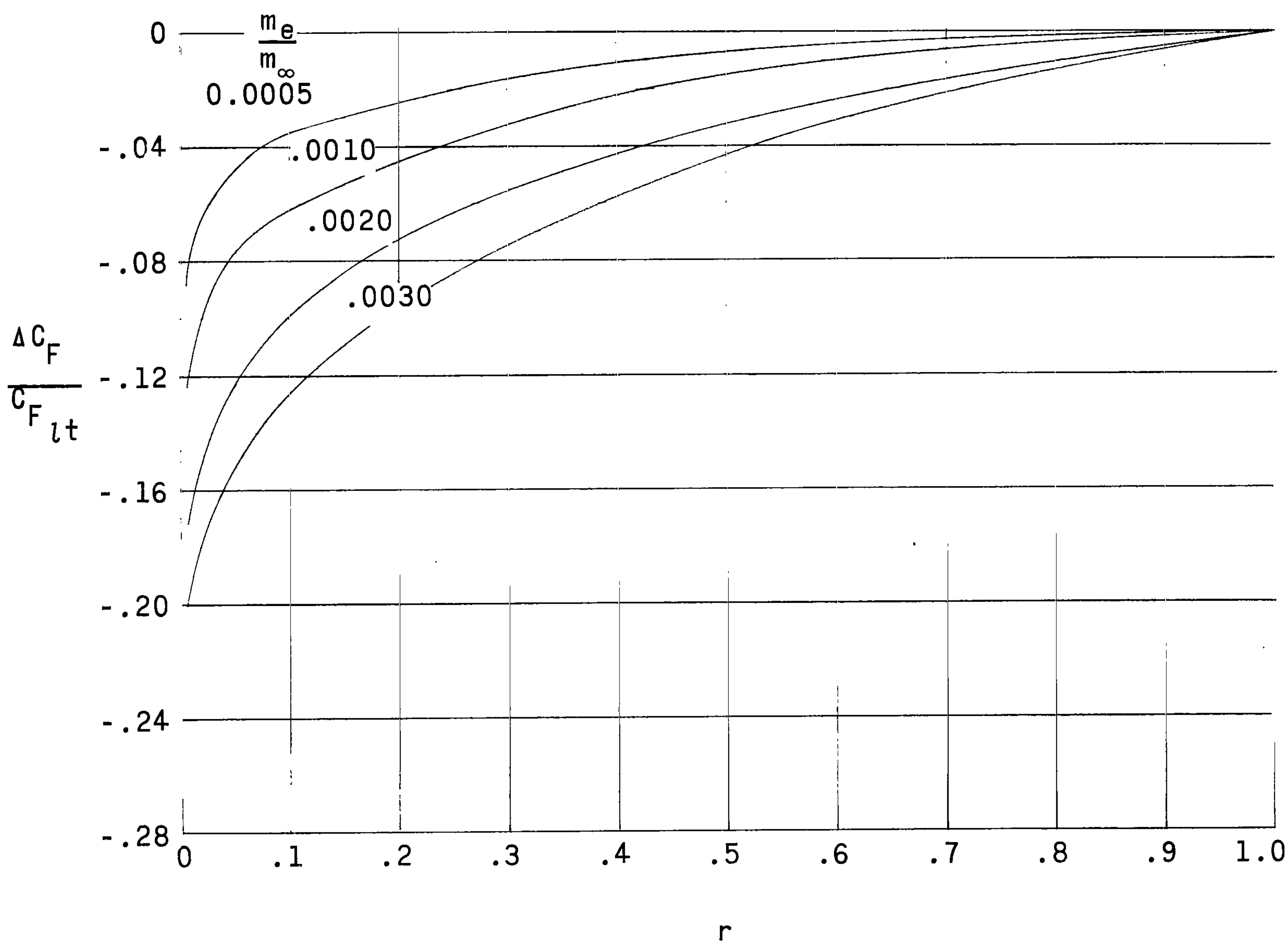

Figure 18.- Effect of $\frac{m_e}{m_\infty}$ on variation of $\frac{\Delta C_F}{C_{F_{lt}}}$ with r. $M_\infty = 3.0$; $R_\infty = 52.5 \times 10^6$; $\frac{T_{t,e}}{T_{t,\infty}} = 1.0$; $\frac{ls}{c} = 0.20$.

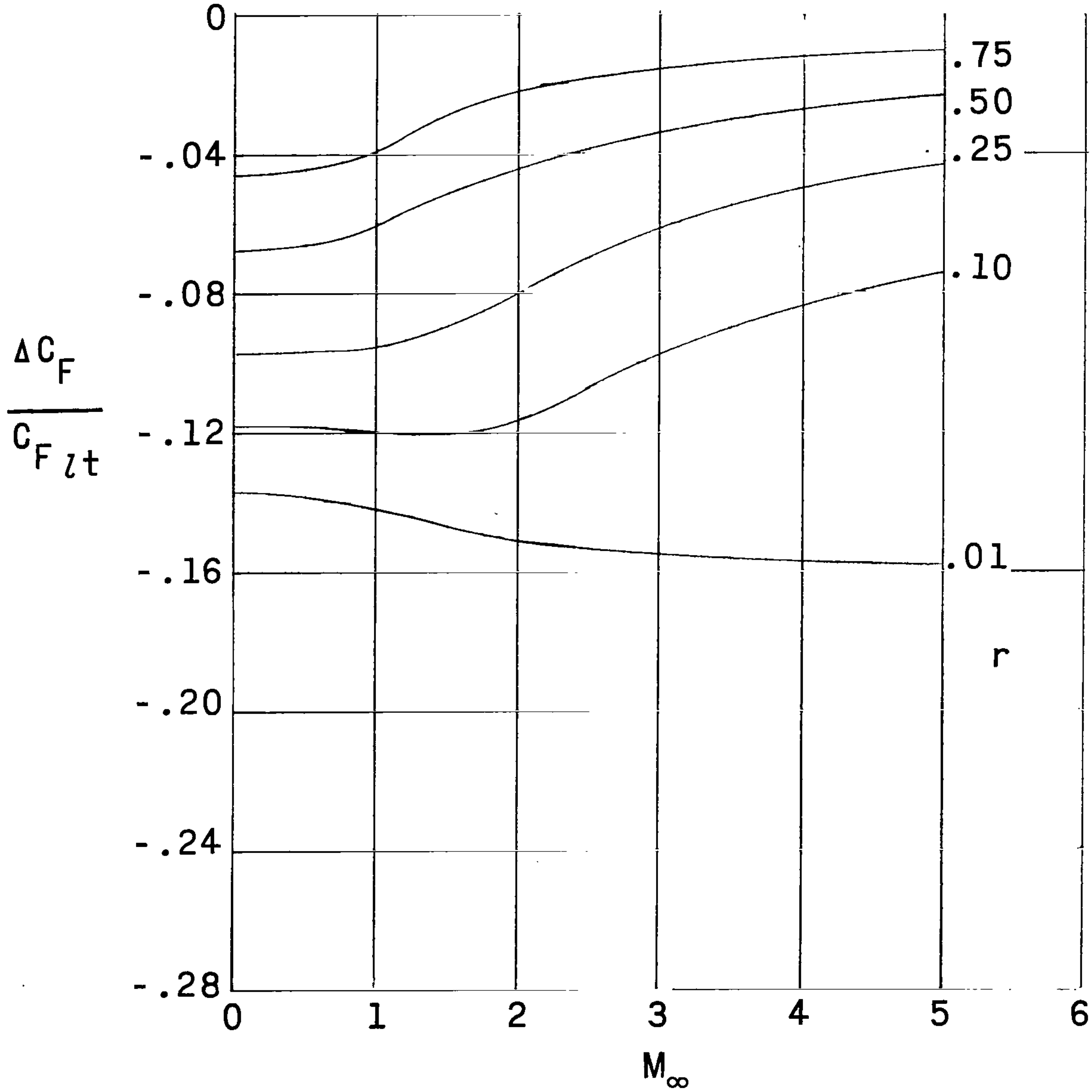

Figure 19.- Variation of $\frac{\Delta C_F}{C_{F_{lt}}}$ with M_∞. $R_\infty = 52.5 \times 10^6$; $\frac{T_{t,e}}{T_{t,\infty}} = 1.0$; $\frac{ls}{c} = 0.20$; $\frac{m_e}{m_\infty} = 0.002$.

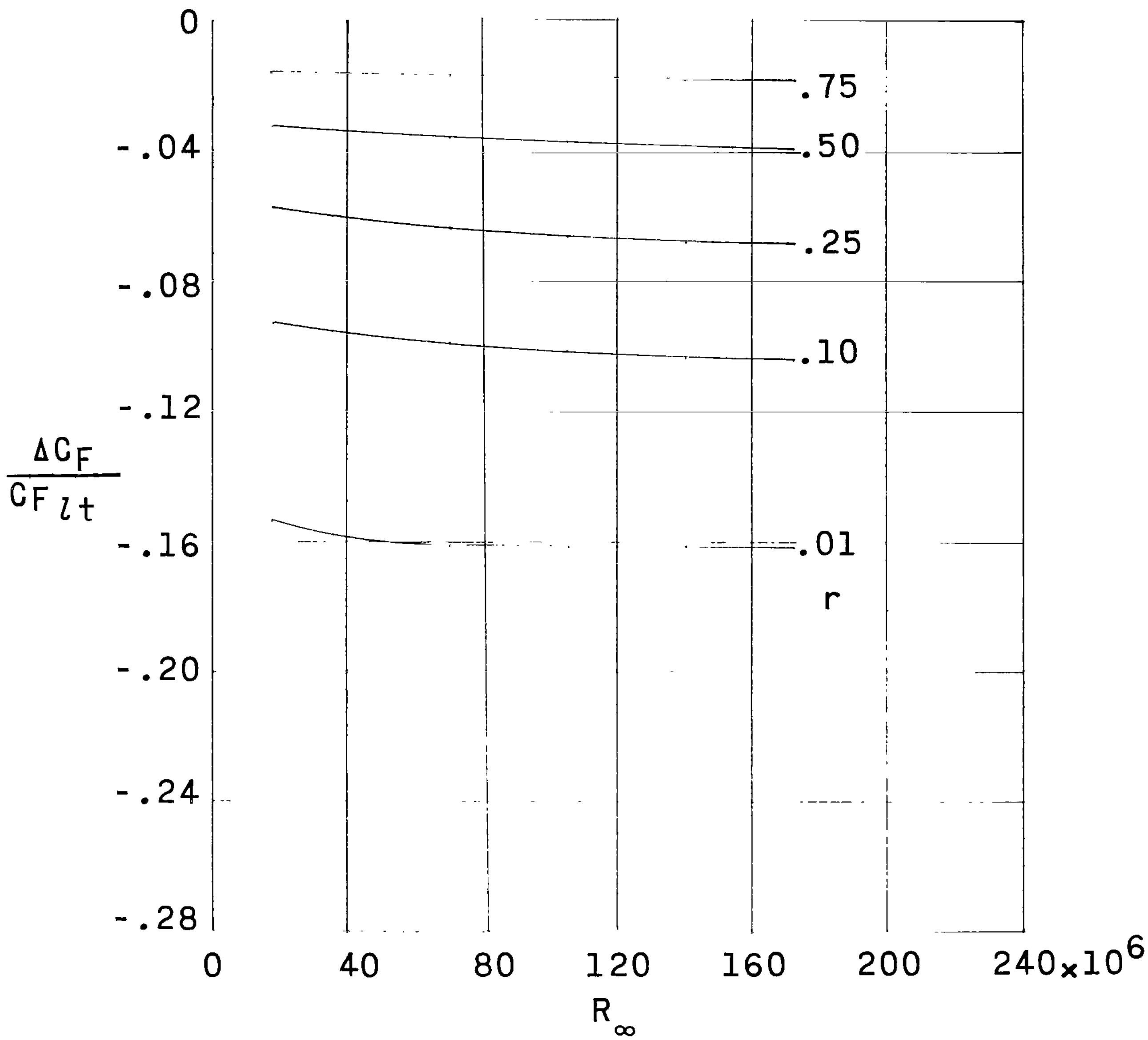

Figure 20.- Variation of $\frac{\Delta C_F}{C_{F_{lt}}}$ with R_∞. $M_\infty = 3.0$; $\frac{T_{t,e}}{T_{t,\infty}} = 1.0$; $\frac{ls}{c} = 0.20$; $\frac{m_e}{m_\infty} = 0.002$.

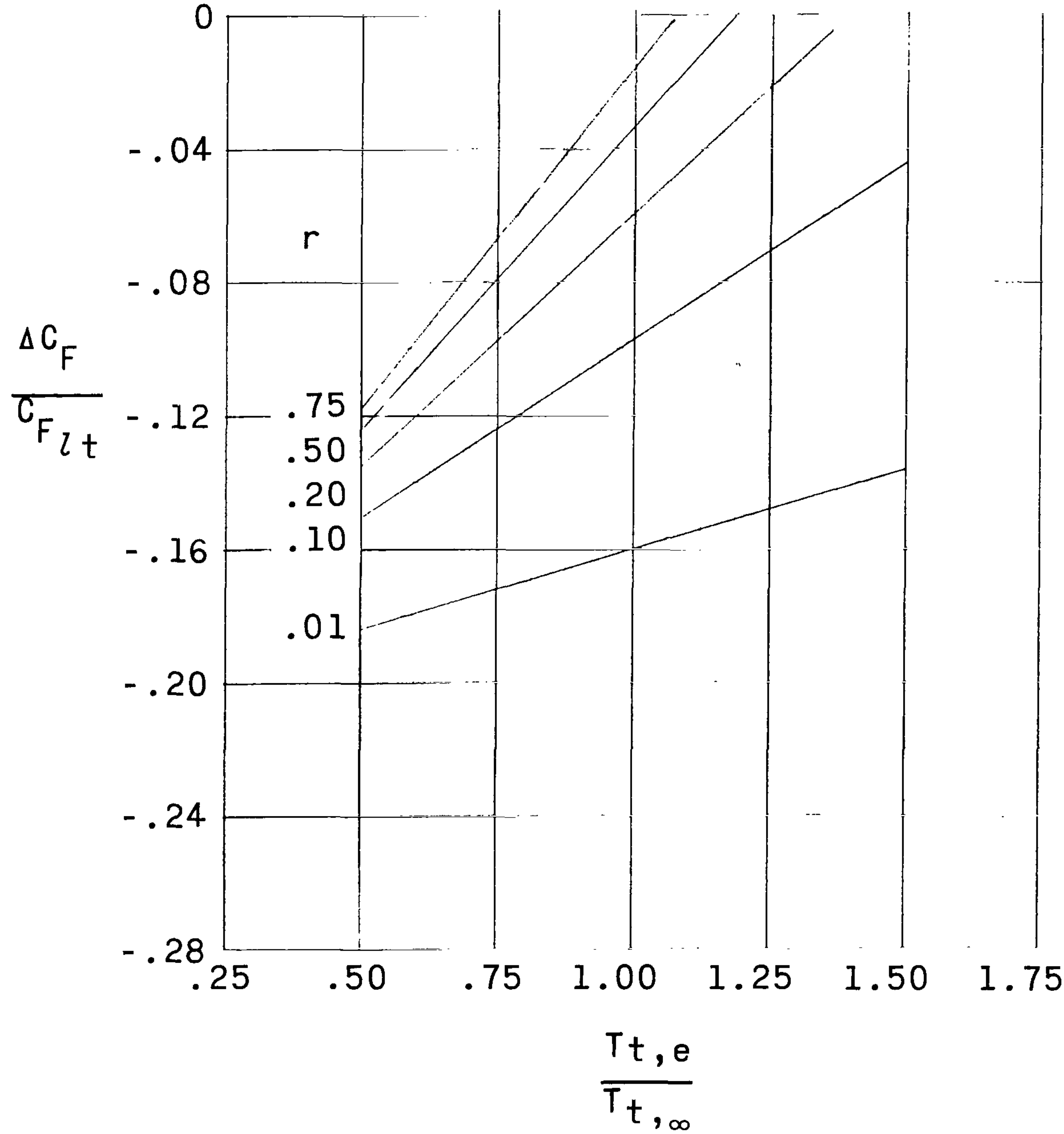

Figure 21.- Variation of $\frac{\Delta C_F}{C_{F_{lt}}}$ with $\frac{T_{t,e}}{T_{t,\infty}}$. $M_\infty = 3.0$; $R_\infty = 52.5 \times 10^6$; $\frac{ls}{c} = 0.20$; $\frac{m_e}{m_\infty} = 0.002$.

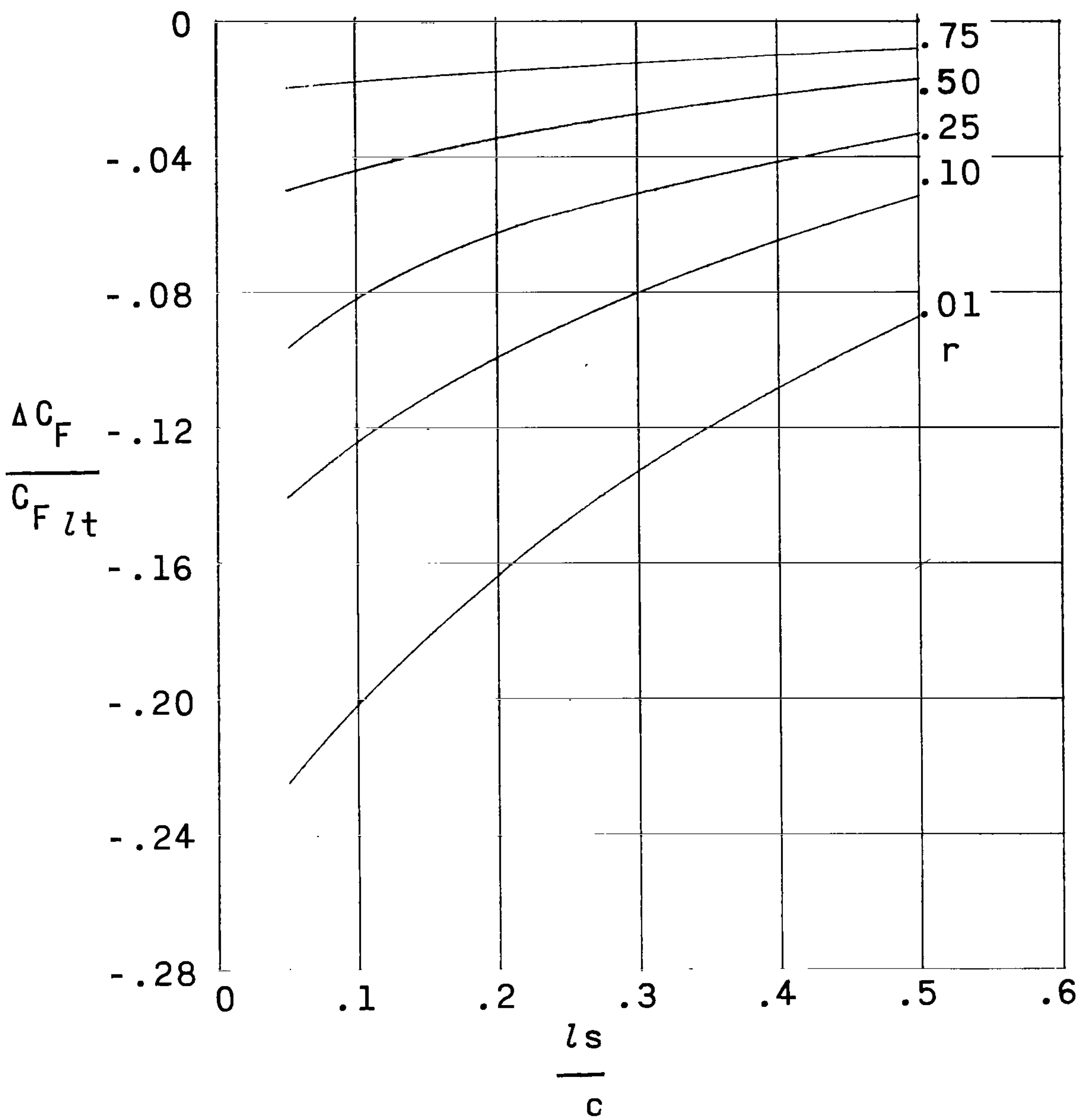

Figure 22.- Variation of $\frac{\Delta C_F}{C_{F_{lt}}}$ with $\frac{ls}{c}$. $M_\infty = 3.0$; $R_\infty = 52.5 \times 10^6$; $\frac{T_{t,e}}{T_{t,\infty}} = 1.0$; $\frac{m_e}{m_\infty} = 0.002$.

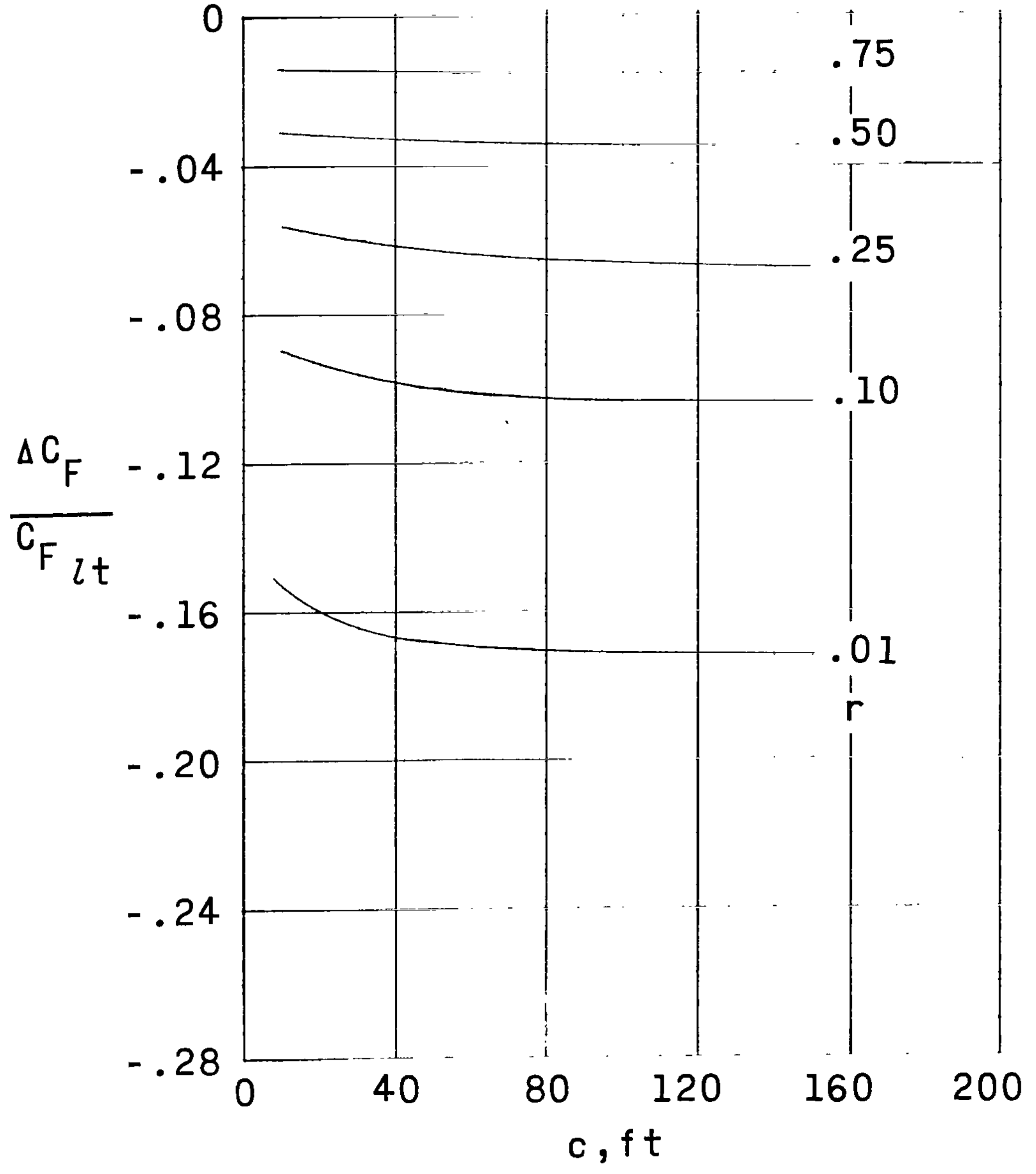

Figure 23.- Variation of $\frac{\Delta C_F}{C_{F_{lt}}}$ with c at a constant $\frac{m_e}{m_\infty}$. $M_\infty = 3.0$; $R_{ft} = 1.5 \times 10^6$; $\frac{T_{t,e}}{T_{t,\infty}} = 1.0$; $\frac{l_s}{c} = 0.20$; $\frac{m_e}{m_\infty} = 0.002$.

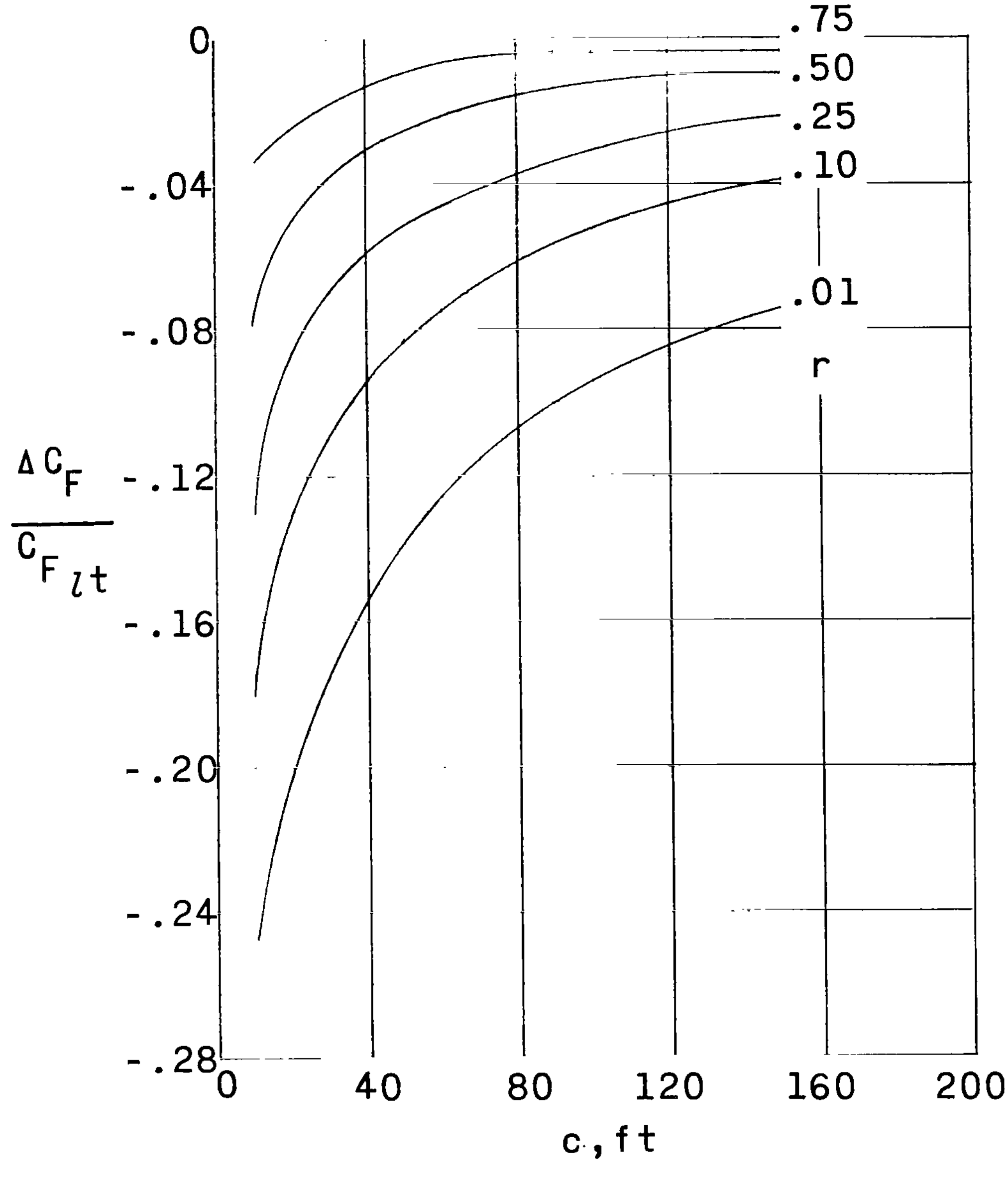

Figure 24.- Variation of $\frac{\Delta C_F}{C_{F_{lt}}}$ with c at constant $\frac{m_e}{m_\infty}\frac{c}{c_{35}}$. $M_\infty = 3.0$; $R_{ft} = 1.5 \times 10^6$; $\frac{T_{t,e}}{T_{t,\infty}} = 1.0$; $\frac{l_s}{c} = 0.20$; $\frac{m_e}{m_\infty}\frac{c}{c_{35}} = 0.002$.

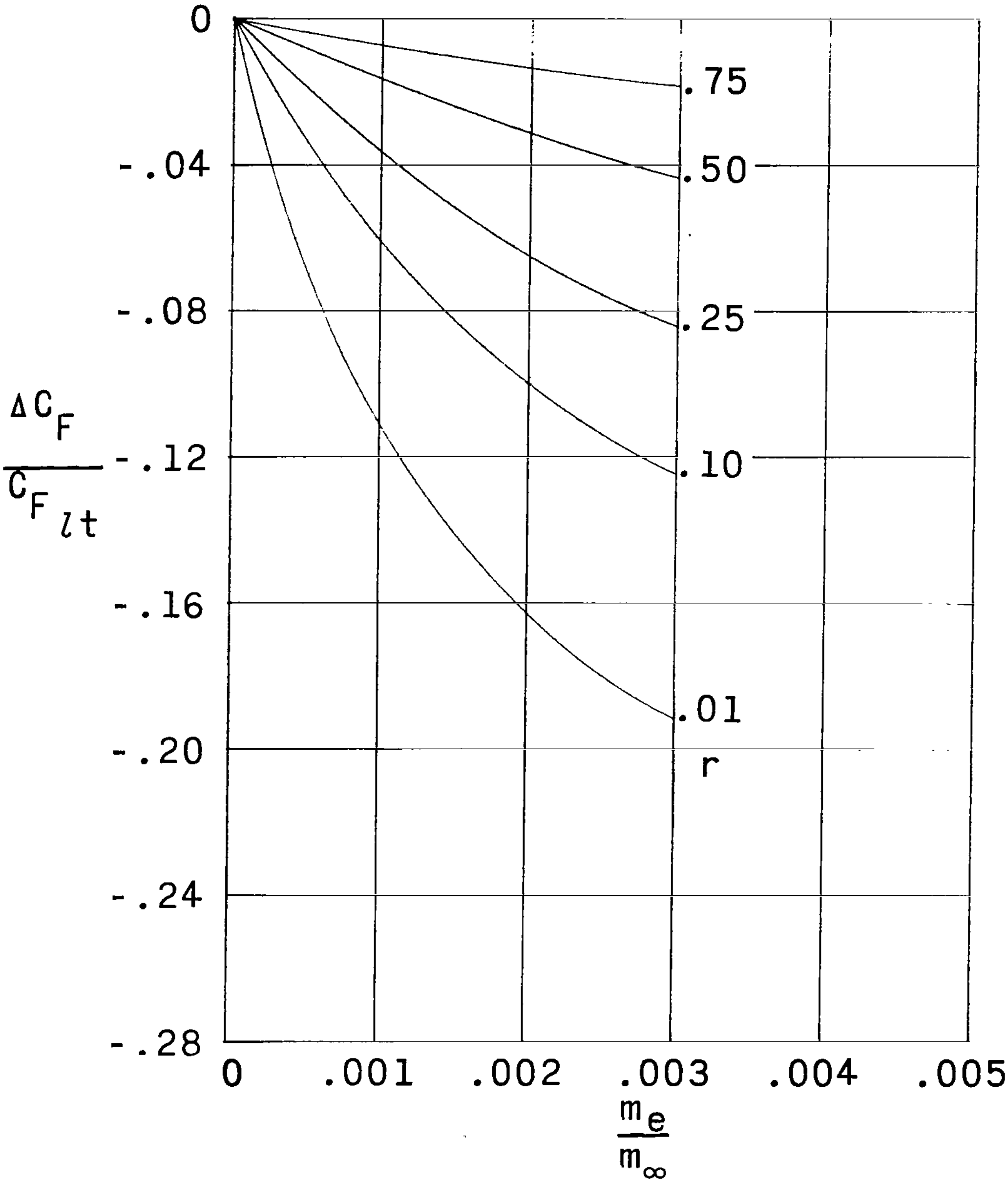

Figure 25.- Variation of $\frac{\Delta C_F}{C_{F_{lt}}}$ with $\frac{m_e}{m_\infty}$. $M_\infty = 3.0$; $R_\infty = 52.5 \times 10^6$; $\frac{T_{t,e}}{T_{t,\infty}} = 1.0$; $\frac{ls}{c} = 0.20$.

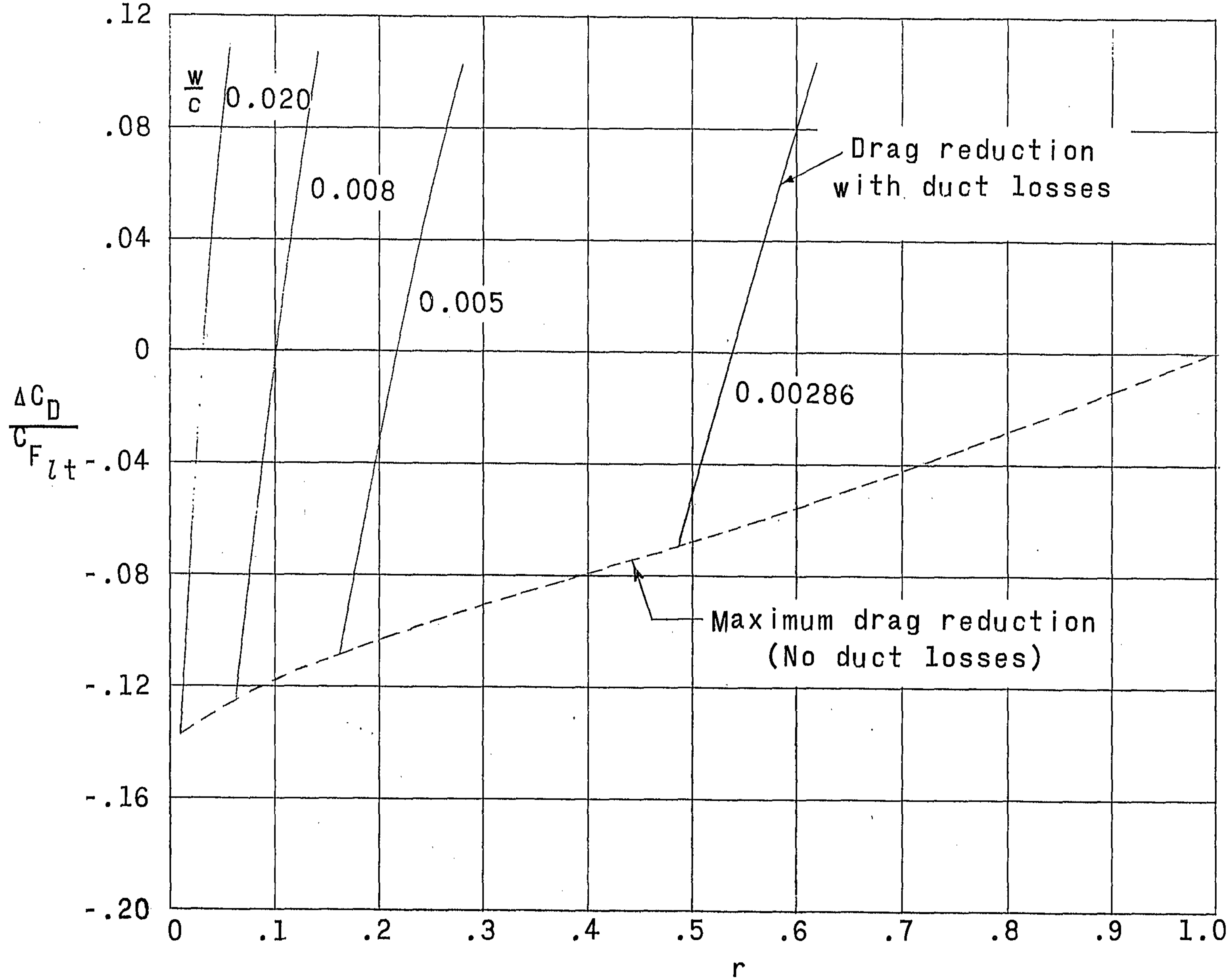

Figure 26.- Effect of duct pressure losses on $\frac{\Delta C_D}{C_{F_{lt}}}$. $M_\infty = 0.1$; $R_\infty = 52.5 \times 10^6$; $\frac{T_{t,e}}{T_{t,\infty}} = 1.0$; $\frac{l_s}{c} = 0.20$; $\frac{m_e}{m_\infty} = 0.002$.

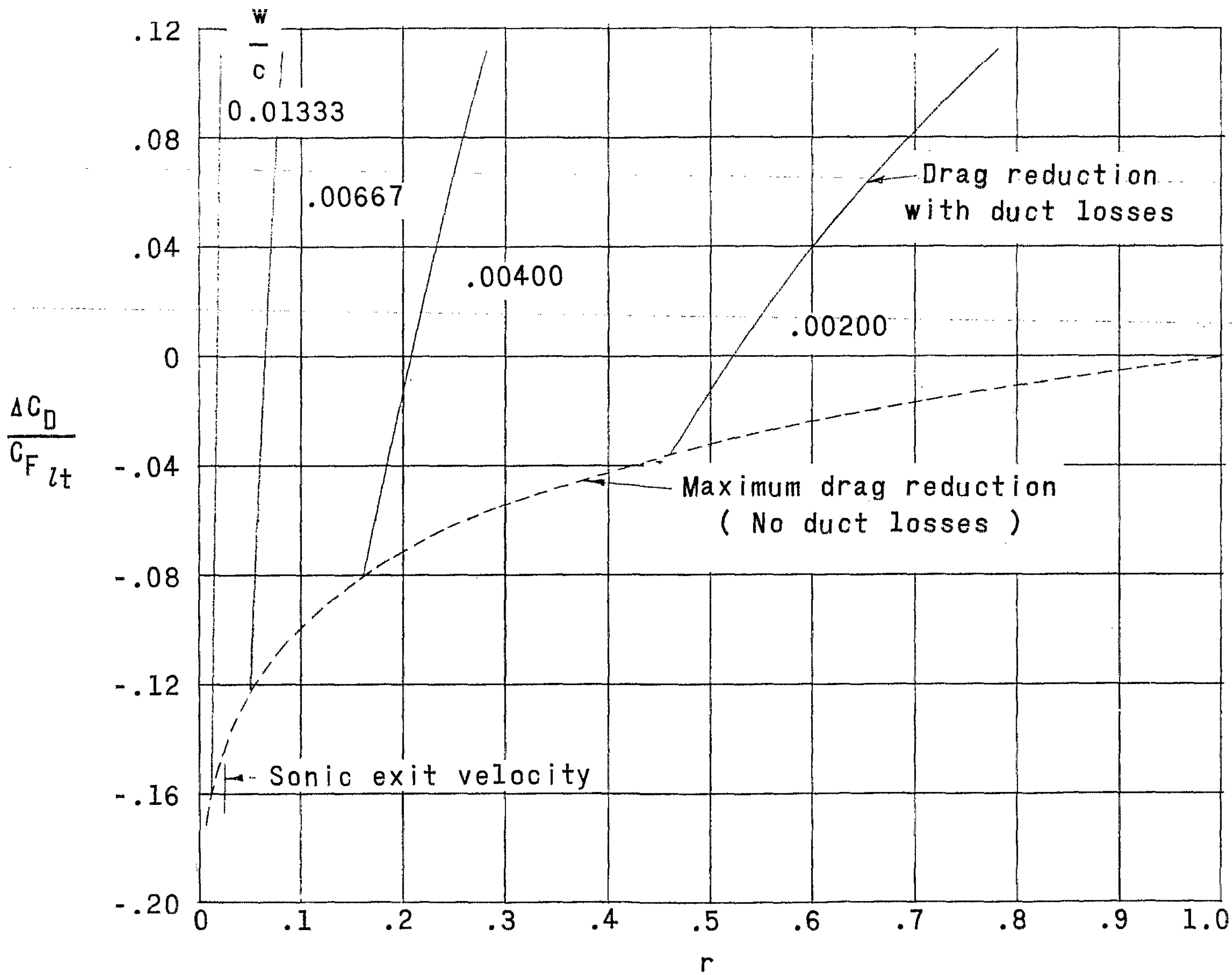

Figure 27.- Effect of duct pressure losses on $\frac{\Delta C_D}{C_{F_{lt}}}$. $M_\infty = 3.0$; $R_\infty = 52.5 \times 10^6$; $\frac{T_{t,e}}{T_{t,\infty}} = 1.0$; $\frac{ls}{c} = 0.20$; $\frac{m_e}{m_\infty} = 0.002$.

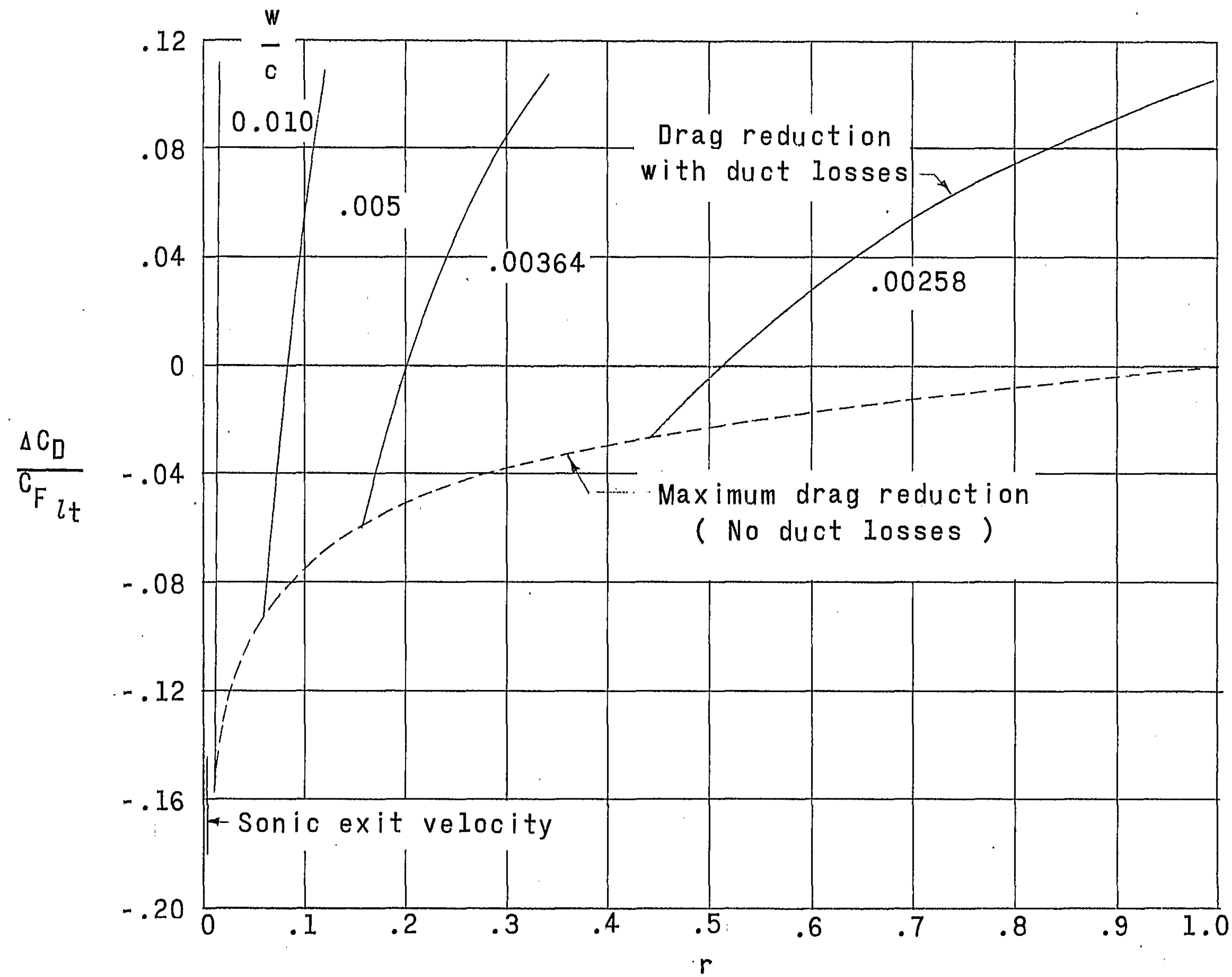

Figure 28.- Effect of duct pressure losses on $\frac{\Delta C_D}{C_{F_{lt}}}$. $M_\infty = 5.0$; $R_\infty = 52.5 \times 10^6$; $\frac{T_{t,e}}{T_{t,\infty}} = 1.0$; $\frac{ls}{c} = 0.20$; $\frac{m_e}{m_\infty} = 0.002$.

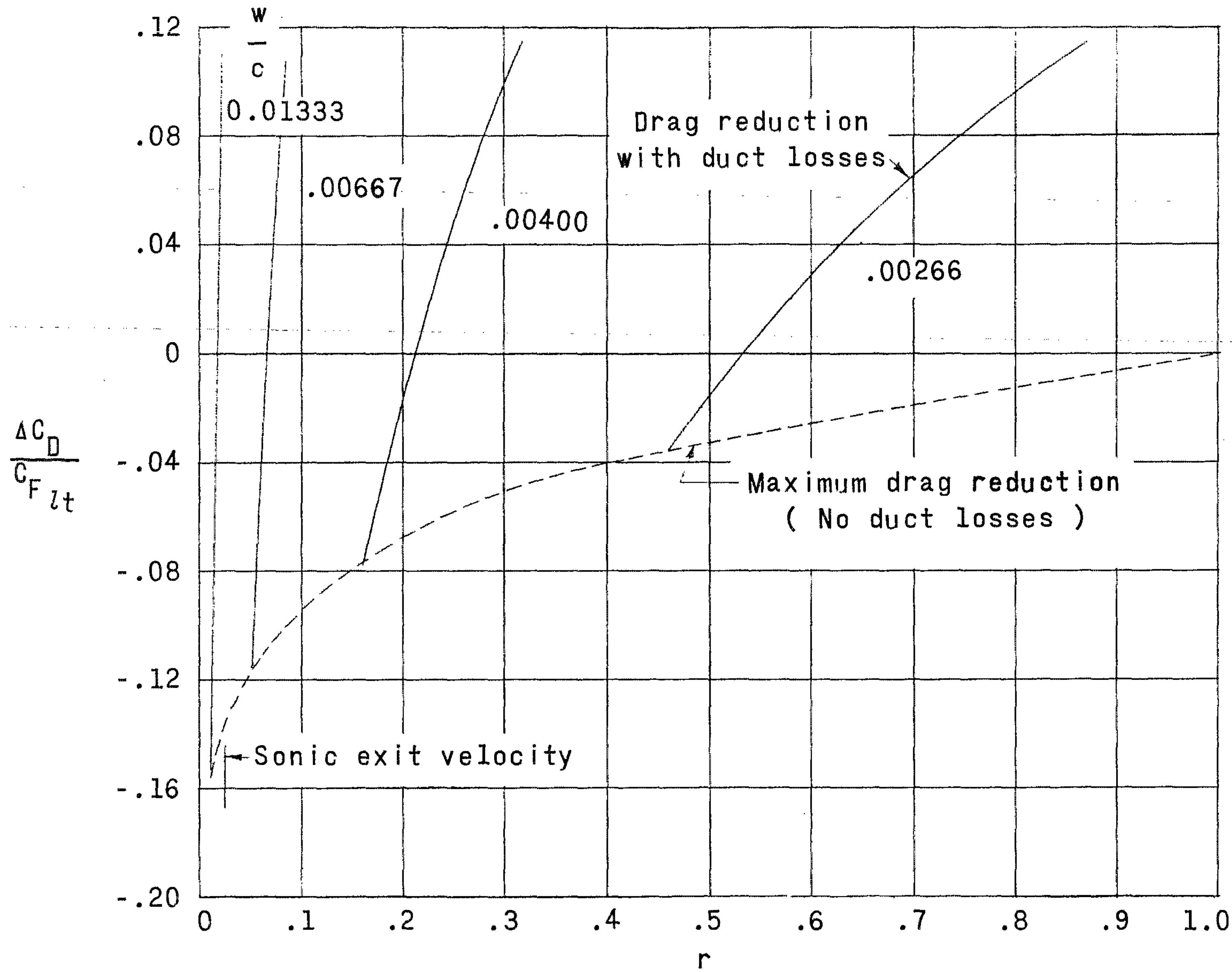

Figure 29.- Effect of duct pressure losses on $\frac{\Delta C_D}{C_{F_{lt}}}$. $M_\infty = 3.0$; $R_\infty = 17.5 \times 10^6$; $\frac{T_{t,e}}{T_{t,\infty}} = 1.0$; $\frac{ls}{c} = 0.20$; $\frac{m_e}{m_\infty} = 0.002$.

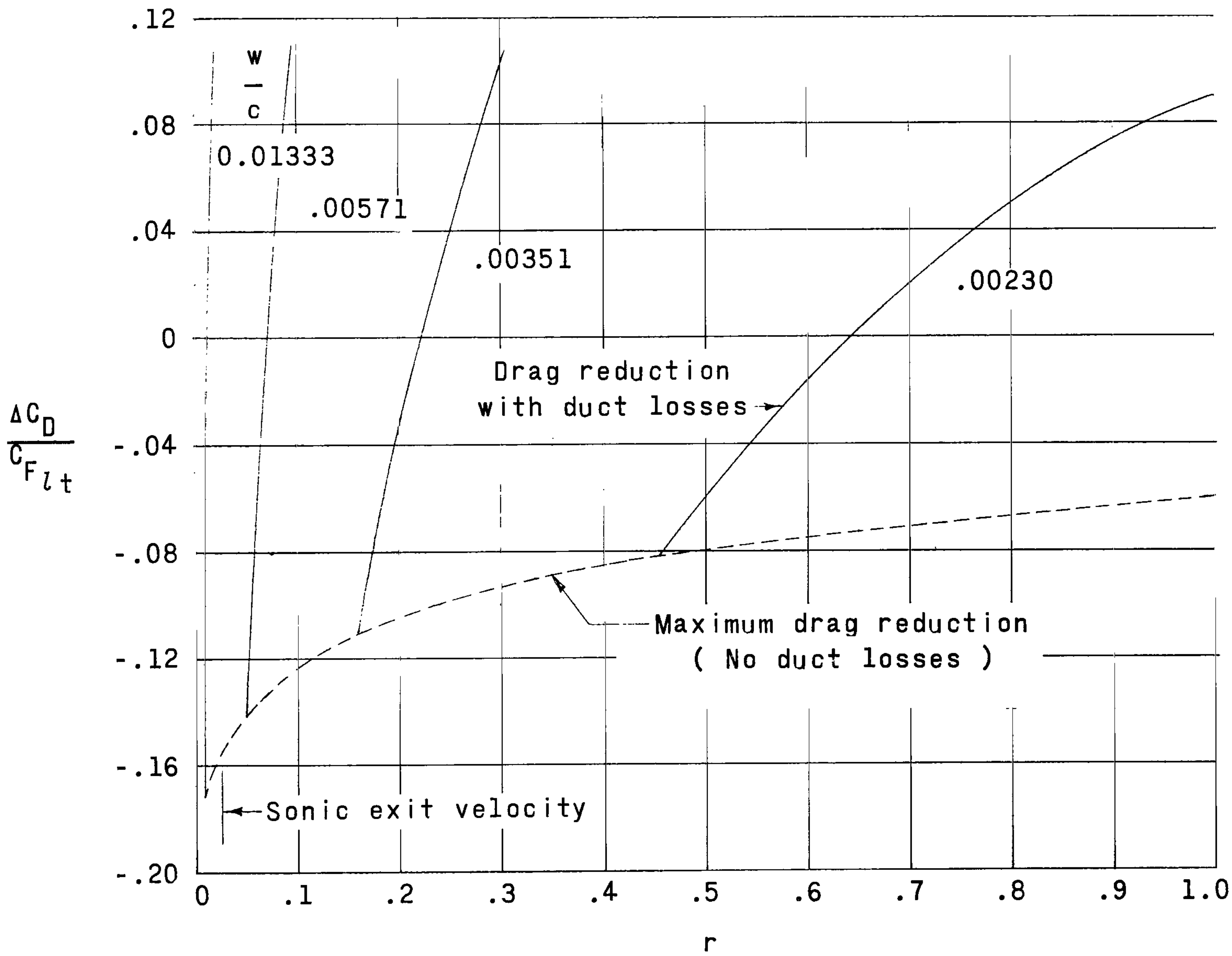

Figure 30.- Effect of duct pressure losses on $\frac{\Delta C_D}{C_{F_{lt}}}$. $M_\infty = 3.0$; $R_\infty = 52.5 \times 10^6$; $\frac{T_{t,e}}{T_{t,\infty}} = 0.75$; $\frac{ls}{c} = 0.20$; $\frac{m_e}{m_\infty} = 0.002$.

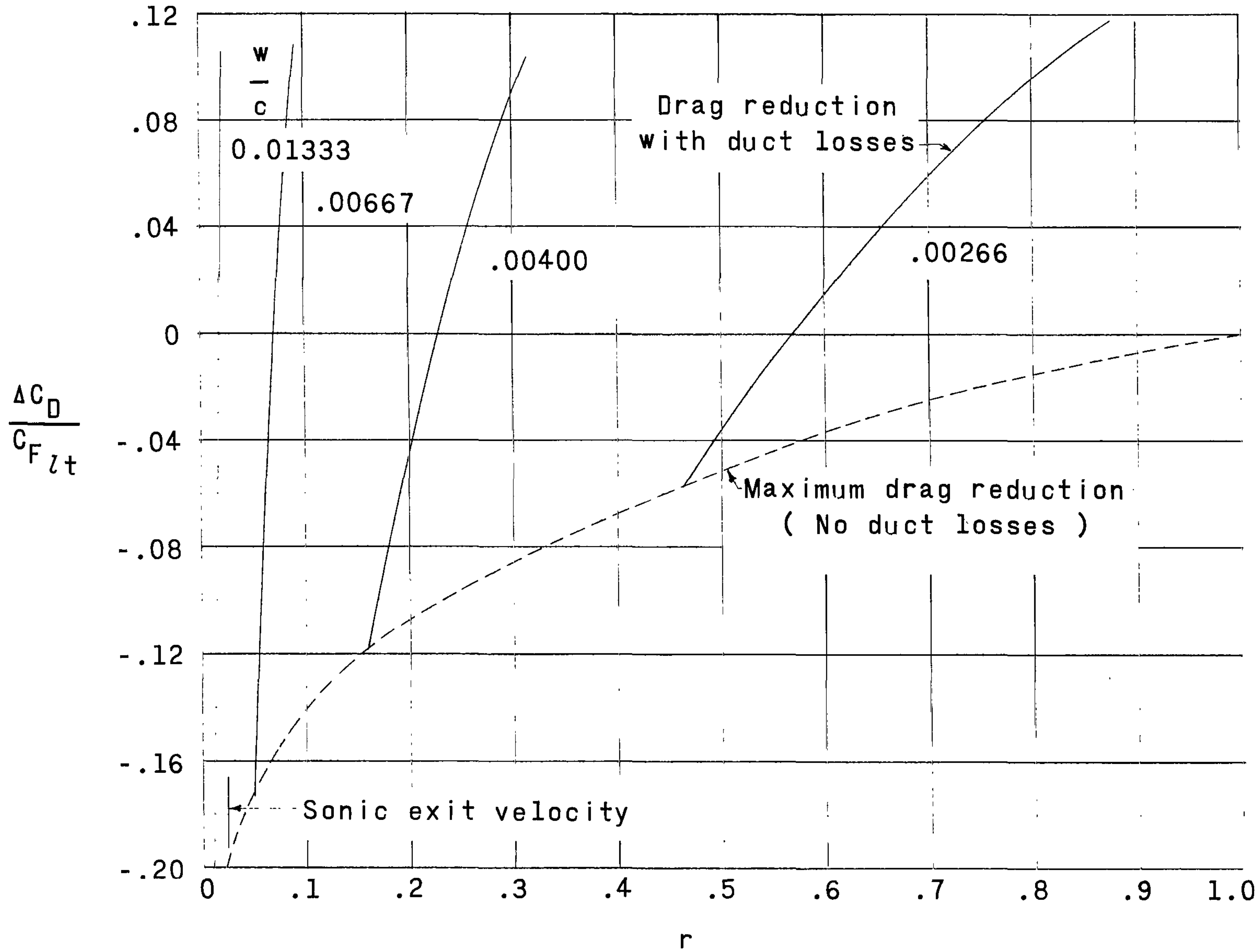

Figure 31.- Effect of duct pressure losses on $\frac{\Delta C_D}{C_{F_{lt}}}$. $M_\infty = 3.0$; $R_\infty = 52.5 \times 10^6$; $\frac{T_{t,e}}{T_{t,\infty}} = 1.0$; $\frac{ls}{c} = 0.005$; $\frac{m_e}{m_\infty} = 0.002$.

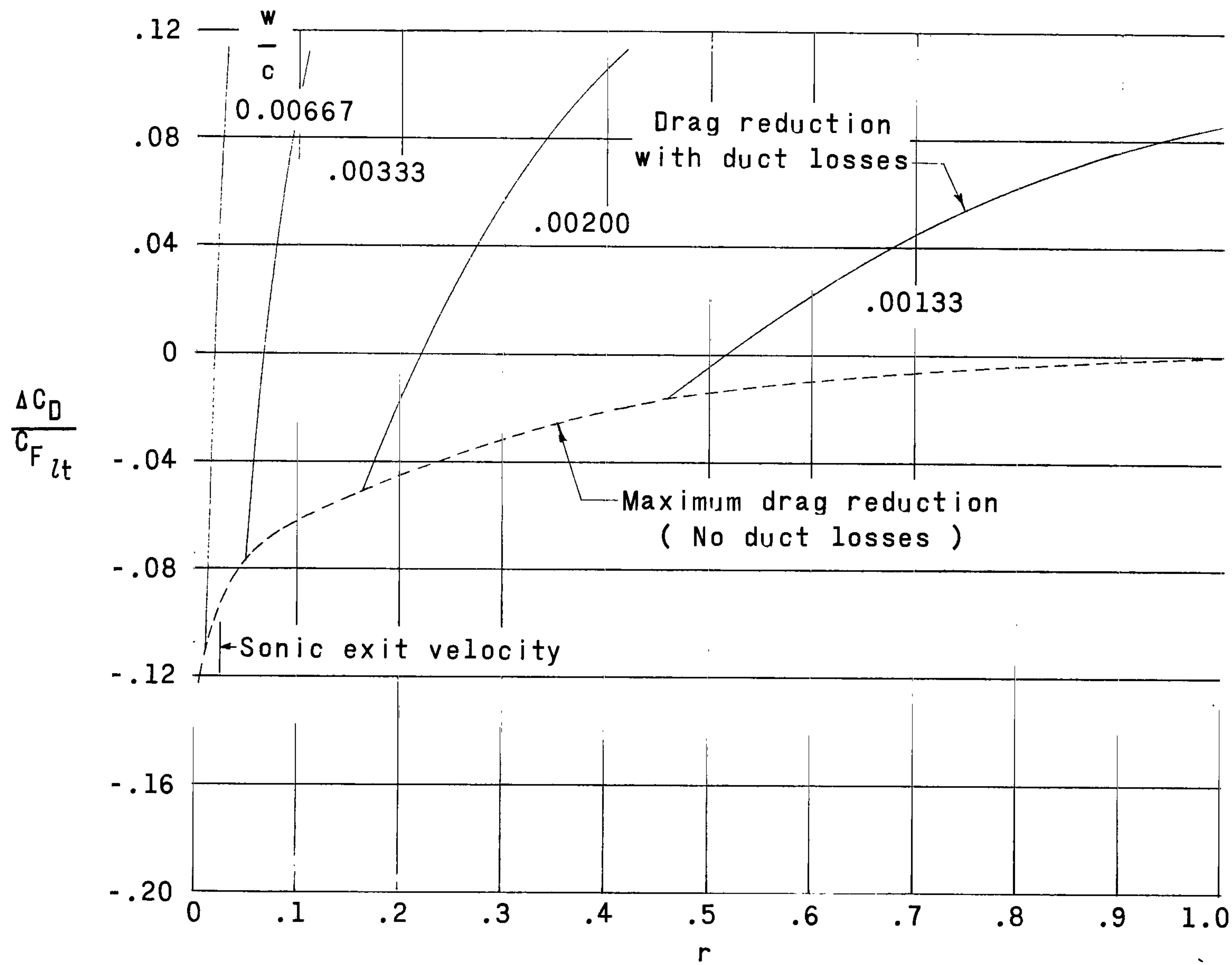

Figure 32.- Effect of duct pressure losses on $\frac{\Delta C_D}{C_{F_{lt}}}$. $M_\infty = 3.0$; $R_\infty = 52.5 \times 10^6$; $\frac{T_{t,e}}{T_{t,\infty}} = 1.0$; $\frac{ls}{c} = 0.20$; $\frac{m_e}{m_\infty} = 0.001$.

NASA-Langley, 1964 L-3988

"The aeronautical and space activities of the United States shall be conducted so as to contribute . . . to the expansion of human knowledge of phenomena in the atmosphere and space. The Administration shall provide for the widest practicable and appropriate dissemination of information concerning its activities and the results thereof."

—NATIONAL AERONAUTICS AND SPACE ACT OF 1958

NASA SCIENTIFIC AND TECHNICAL PUBLICATIONS

TECHNICAL REPORTS: Scientific and technical information considered important, complete, and a lasting contribution to existing knowledge.

TECHNICAL NOTES: Information less broad in scope but nevertheless of importance as a contribution to existing knowledge.

TECHNICAL MEMORANDUMS: Information receiving limited distribution because of preliminary data, security classification, or other reasons.

CONTRACTOR REPORTS: Technical information generated in connection with a NASA contract or grant and released under NASA auspices.

TECHNICAL TRANSLATIONS: Information published in a foreign language considered to merit NASA distribution in English.

TECHNICAL REPRINTS: Information derived from NASA activities and initially published in the form of journal articles.

SPECIAL PUBLICATIONS: Information derived from or of value to NASA activities but not necessarily reporting the results of individual NASA-programmed scientific efforts. Publications include conference proceedings, monographs, data compilations, handbooks, sourcebooks, and special bibliographies.

Details on the availability of these publications may be obtained from:

SCIENTIFIC AND TECHNICAL INFORMATION DIVISION

NATIONAL AERONAUTICS AND SPACE ADMINISTRATION

Washington, D.C. 20546